GRAZ UNIVERSITY OF TECHOLOGY

MASTER THESIS

Design and Characterization of Microstrip Structures at mm-wave Frequencies

Author:

Sebastian Wolfgang SATTLER
B.Sc.

Supervisor:

Dipl.-Ing. Dr.techn.
Michael GADRINGER

A thesis submitted in fulfilment of the requirements
for the degree of Master of Sciences

in the

Microwave Technologies Group
Institute of Microwave and Photonic Engineering

November 2015

Declaration of Authorship

Ich erkläre an Eides statt, dass ich die vorliegende Arbeit selbstständig verfasst, andere als die angegebenen Quellen/Hilfsmittel nicht benutzt, und die den benutzten Quellen wörtlich und inhaltlich entnommenen Stellen als solche kenntlich gemacht habe. Das in TUGRAZonline hochgeladene Textdokument ist mit der vorliegenden Masterarbeit/Diplomarbeit identisch.

I declare that I have authored this thesis independently, that I have not used other than the declared sources/resources, and that I have explicitly indicated all material which has been quoted either literally or by content from the sources used. The text document uploaded to TUGRAZonline is identical to the present doctoral dissertation.

Signed:

Date:

GRAZ UNIVERSITY OF TECHNOLOGY

Abstract

Faculty of Electrical and Information Engineering
Institute of Microwave and Photonic Engineering

Master of Sciences

by Sebastian Wolfgang SATTLER B.Sc.

Applications nowadays ask for higher data rates, which can be achieved by increasing the bandwidth or by switching to a higher order modulation scheme. Using a higher order modulation scheme however, reduces the signal to noise ratio and since a lot of applications occupy the specified frequency spectrum, it is not possible to increase the signal power because that would also mean a higher noise level for other applications using this frequency band. The mass of applications being cramped in the known frequency spectrum right now also explains why the bandwidth can not be increased without interfering with other users of this frequency spectrum. The solution is the step to mm-wave frequencies to satisfy the demand for higher data rates. However the design of mm-wave structures is not straight forward and requires a lot of information about the behavior of the structure and the characteristics of the circuit board itself.

This thesis aims to create a design that enables the measurement and therefore characterization of mm-wave structures. The devices and structures investigated in the framework of this thesis are part of a research project on building a mm-wave RFID demonstrator. This application requires the profound knowledge of the device behavior composing the demonstrator in the mm-wave regime as well as at the baseband. To provide the required information vector network analyzer measurements have to be performed of the circuit elements located on a printed circuit board (PCB) . Therefore, calibration standards for non-coaxial measurement have to be derived. Deriving these measurement standards for the frequency range below $3\,\mathrm{GHz}$ is one of the main aspects of this thesis.

Another important issue are the mm-wave measurements. These are advantageously accomplished for an on-wafer prober setup. Even if this measurement approach is widely used for measuring integrated circuit, the probing of mm-wave PCBs shows its own demands. Especially the design of the PCB interface for the probes has an significant influence on the performance of the desired measurements. The optimization of the design of these launches is the second key aspect of this thesis.

Kurzfassung

Heutige Anwendungen verlangen nach immer höheren Datenraten, die man durch Vergrößerung der Bandbreite, oder durch Erhöhung der Ordnung der Modulationsart erreichen kann. Erhöht man die Ordnung des Modulationsverfahren, verringert man aber gleichzeitig auch den Störabstand. Man kann auch nicht einfach die Signalleistung erhöhen, da andere Anwendungen dasselbe Frequenzspektrum benützen und es für diese eine Erhöhung des Rauschpegels wäre. Die große Anzahl an Anwendungen, die alle in dasselbe Frequenzband gezwängt werden, erklärt auch, wieso man nicht die Bandbreite erhöhen kann ohne andere Benützer des Frequenzbandes zu stören. Die Lösung ist der Wechsel zu mm Wellen Frequenzen um das Verlangen nach höheren Datenraten zu stillen. Allerdings ist das Design von mm Wellen Strukturen nicht einfach und benötigt sehr viel Information über das Verhalten der Struktur und die Eigenschaften der Platine.

Diese Masterarbeit zielt darauf ab ein Design zu kreieren, dass es ermöglicht mm Wellen Strukturen zu messend und damit auch zu charakterisieren. Die Geräte und Stukturen, die im Rahmen dieser Arbeit betrachtet werden, sind Teil eines Forschungsprojekts zum Bau eines mm Wellen RFID Demonstrators. Diese Anwendung verlangt nach hochgradigem Wissen über das Verhalten der Gerätekomponenten des Demonstrators im mm Wellen Frequenzband und im niederfrequenten Basisband. Um diese Informationen zu erhalten müssen Vector Netzwerk Analysator Messungen an Bauelementen auf Leiterplatten (PCB) durchgeführt werden. Dafür müssen nicht koaxiale Kalibrationsstandards hergeleitet werden. Die Herleitung dieser Messstandards für Frequenzen unter 3 GHz ist einer der Hauptaspekte dieser Arbeit.

Ein weiterr Aspekt sind die mm Wellen Messungen. Ein Wafer-Prober setup erweist sich hierbei als vorteilhaft. Auch wenn dieser Messansatz weit verbreitet für die Messung integrierter Schaltungen ist, weißt das Testen von mm Wellen PCBs höhere Ansprüche auf. Im Speziellen hat das Design vom Interface zwischen Probe und PCB einen großen Einfluss auf das Verhalten der gewünschten Messungen. Die Optimierung des Designs von diesen Launches ist der zweite Hauptaspekt dieser Masterarbeit.

Acknowledgements

I would like to thank my two supervisors, Dipl.-Ing. Dr.techn. Michael Ernst Gadringer and Dipl.-Ing. Philipp Franz Freidl for their support and knowledge input they provided during the time of my employment.

Contents

List of Figures

List of Tables

Chapter 1

Introduction

This thesis has its focus on how to characterize and realize microwave structures at mm wave frequencies. These structures will then be used to design a radio frequency front-end for a mm wave RFID transponder.

This chapter includes the motivation of the project and the whole structure of the thesis.

1.1 Motivation

The goal of this master thesis is to create designs of launches at mm-wave frequencies that enable the measurement and characterization for mm-wave structures. These structures are part of a research project to build a mm-wave RFID demonstrator. At mm-wave frequencies the designing of even simple microwave structures such as transmission lines is not straight forward, due to the fact that even small deviations within the used materials and the tolerances of the fabrication itself can cause major differences between the expected and the real behaviour of the transmission line. Therefore the reduction of the launches affecting the measurement of the microwave structures is a key aspect of this thesis.

Another aspect is to gain a deeper understanding of measurement and calibration itself. Therefore the second key part of the thesis is the design and the evaluation of a calibration-kit for frequencies below $3\,\mathrm{GHz}$.

1.2 Structure of the Thesis

First this thesis will give a short introduction to RFID and as to why it is beneficial to switch to mm-wave frequencies.

The next part describes the theory behind measuring structures at high frequencies and why the measurement equipment has to be calibrated to provide meaningful measurement results.

The third part contains the design of a calibration-kit for frequencies up to 3 GHz. Beginning with the choice of the calibration method and simulation of a simple structure, followed by the layout and the measurement results.

The launch at a PCB providing the connection to the on-wafer measurement system is a key component for device characterization at 74 GHz. Its design and optimized layout is derived in the last chapter.

Chapter 2

RFID at mm-wave Frequencies

2.1   Basics of RFID

RFID (**R**adio **F**requency **I**dentification) finds its use in an enormous amount of nowadays applications, mainly in logistics and sensors [1]. A RFID base station uses electromagnetic waves (the RF part of RFID), which enables a contact-less energy and data transmission to identify a RFID chip (transponder) in its vicinity. Time-tested applications are for example article surveillance in department stores and replacement/supplement of bar codes in supermarkets, with rather simple and therefore cheap RFID chips on the one hand and automatic toll services on highways or the new generation of passports with secure, more complex RFID chips on the other.

A RFID system usually contains a reader and a transponder/tag illustrated in Figure 2.1.
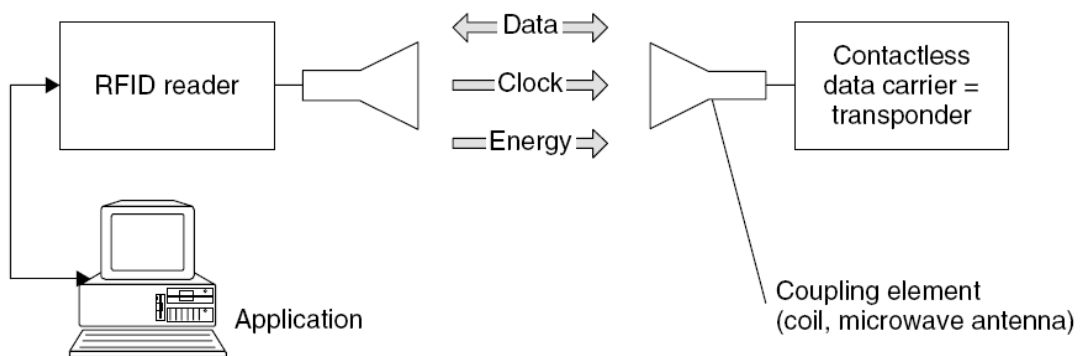
FIGURE 2.1: RFID Components [1]

3

- **Reader**

  The reader provides the electromagnetic field necessary for the interaction with the transponder. It is also communicating with the application interface which could be a database or simply a speaker which sounds an alarm if the transponder is removed from a certain area.

- **Transponder/Tag**

  The Tag is only interacting with the reader and stores the desired information. Whether its a simple "I am here" or a complex data transmission, depends on the application. Possible communication schemes are load modulation or back-scatter for passive transponders.

For the reader and transponder to interact with, an emitted electromagnetic field at either high or low frequency is needed. Transponders in the proximate vicinity of the reader up to a range of 1 m use either the principle of inductive coupling or the principle of electromagnetic waves. Long range systems (r >1 m) solely use the principle of electromagnetic wave propagation [1].

2.1.1 Fundamental Physical Principles

For the reader and transponder to communicate there has to be a physical connection which is an alternating electromagnetic field for the RFID case. Due to the properties of this field there is a distinction between the so called Reactive Near-Field, Radiating Near-Field and the Far-Field (see Figure 2.2). Two main principles are used to establish a connection between the reader and the transponder [1].

- **Inductive Coupling**

  The principle of inductive coupling is possible in the Reactive Near-Field ($r < \dfrac{\lambda}{2\pi}$, r is the distance between reader and transponder) of the antenna. In this area magnetic and electric field components are existent but are not orthogonal to each other. In case of inductive coupling, the alternating magnetic field emitted by the reader antenna (often a loop antenna) induces a voltage in the transponder antenna, which is used for the operation of the transponder.

- **Electromagnetic Waves**

  In the Far-Field ($r > \dfrac{2D^2}{\lambda}$, D is the dimension of the antenna) the electric and magnetic field lines are orthogonal and do not point in the radiating direction. The reader radiates an electromagnetic wave (P_T) towards the transponder which reflects a power proportional to the power density at the transponder. The range
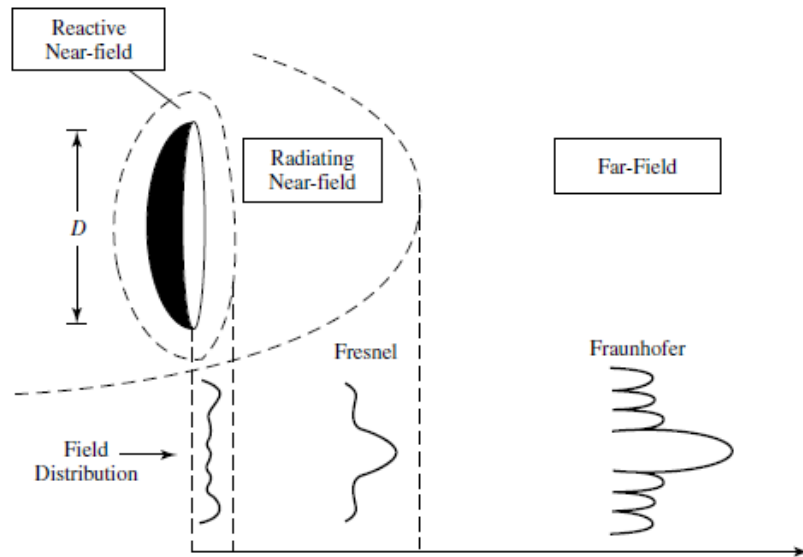
FIGURE 2.2: Field Regions [2]

of such a system is limited by the fast decaying power density (free space loss $\frac{1}{4\pi R^2}$) for passive systems [1].

$$P_R = P_T \cdot G_{Ant} \cdot A_{Ant} \cdot \frac{1}{(4\pi \cdot R^2)^2} \cdot \Gamma \tag{2.1}$$

P_R is the received Power at the reader, G_{Ant} is the antenna gain of the reader antenna and A_{Ant} is the effective antenna area ($A_{ANT} = \frac{\lambda^2}{4\cdot\pi} \cdot G_{Ant}$). The transponder changes the reflection coefficient Γ to communicate with the reader. The free space loss appears in the forward and the reverse communication direction [1].

2.1.2 Transponder Power Supply

There are three different kinds of transponders:

- **passive**

  A passive transponder is solely supplied by the alternating electromagnetic field emitted by the reader. Therefore a data transmission between reader and transponder is only possible, if the transponder is within the readers range. This range is determined by the emitted energy of the reader which has to be enough to supply the transponder with sufficient power to operate. That means the power density at the transponders antenna has to be enough to supply the transponder [1].

- **semi passive**

  Semi-passive transponders usually have a small battery to power the microchip

needed for a data transmission. They do not generate their own response signal but modulate the incoming one (back-scatter). Because these kind of transponders do not need the emitted energy of the reader to power the microchip, the range of such a system is higher than that of a passive transponder. However it is also more expensive and therefore used to track and identify more expensive objects [1].

- **active**
  An active transponder has its own power source and also generates its own response signal. Therefore the range and complexity of such a system is even higher than that of a semi-passive transponder [1].

2.1.3   Frequency Bands

Different frequencies have different benefits when it comes to for example noise sensitivity, range and data transfer speed. Different frequencies also use different transmission principles.

- **LF**
  Low Frequency ranging from 30 kHz to 300 kHz. Low frequency systems are usually short range ($r < 1\,m$) and have low data rates, but are robust and cheap. Applications are for example inventory control and admission control. 125 kHz is the main frequency used within the LF range [1].

- **HF**
  High Frequency ranging from 300 kHz to 30 MHz. Systems in this frequency range have middle to high data rates and ranges beyond 10 cm. The main frequency utilized in this frequency range is 13.56 MHz. One application are the so called Smart Cards. These cards usually have the size of a credit card. They are used for identification purposes as well as for contact-less payment [1].

- **UHF**
  Ultra High Frequency ranging from 30 MHz to 3 GHz. UHF systems have a high reading rate and a long range (up to 6 m for passive and 100 m for semi-passive transponders). These long ranges can lead to misinterpretation at the reader due to reflections. Frequencies used within the UHF range are 867-869 MHz, 902-928 MHz and 2.45 GHz. These tags are mainly utilized in the range of logistics and auto-mobile applications [1].

- **Microwave** Microwave Frequency ranging from 3 GHz up to 30 GHz. Ranges up to 6 m with semi-passive transponders but higher data rates. Such tags are especially for auto-mobile applications due to the high reading rates [1].

- **mm-wave**
  Frequencies beyond 30 GHz are not yet utilized for known RFID applications. The topic of mm-wave frequencies is under research.

2.1.4 Data Transfer Transponder to Reader

There are three main principles for the transponder to be able to respond to a request of a reader.

- **Sub-harmonics**
  The transponder responds at a different frequency which is derived of an integer division of the reader request signal frequency. A binary divider on the transponder chips performs this task. The output signal can the be modulated with the desired data stream [1].

- **load modulation**
  The transponder influences the reader request signal by changing its load. Due to the load change more or less energy is send back to the reader which affects the received signals amplitude on the reader side. Load modulation is used with the physical principle of inductive coupling [1].

- **Back-scatter**
  Similar to the load modulation scheme, the back-scatter scheme influences the received signal energy at the reader. The difference between load modulation and back-scatter is the physical principle. Back-scatter uses the principle of electro-magnetic waves and changes the back-scattering cross-section of the transponder [1].

2.2 Transition to mm-waves

RFID systems at micro-wave frequencies (for example at $5.8\,\text{GHz}$) are already well established and running. However applications nowadays call for higher data-rates which are available at higher frequencies than those which are already in common use, since the data-rate C of a channel is given by the bandwidth B and signal to noise ratio SNR which is available for said channel (2.2).

$$C = B \cdot ld(1 + SNR) \tag{2.2}$$

Due to more and more applications flooding the available frequency spectrum it is not possible to for one application to have lots of bandwidth without interference from another application. For example an application with a carrier frequency of 2 GHz and in need of 2 GHz bandwidth would interfere with WLAN, Bluetooth and various other applications. Changing the carrier frequency to mm-wave frequencies creates the possibility of broadband channels without interference of other channels simply because the relative bandwidth is much smaller compared to the same bandwidth used at lower frequencies. For example 2 GHz absolute bandwidth would be 100% relative bandwidth at a carrier frequency of 2 GHz but only 4% relative bandwidth at a carrier frequency of 50 GHz.

Another benefit is the faster decaying signal strength due to a higher path-loss. The benefit being that systems with the same carrier frequency can operate relatively close to each other without interfering the other systems. Therefore the next step in radio communications is to make this frequency spectrum available for such applications which will not only be RFID systems. To create a working system in this frequency range is unfortunately not as straight forward as it is in lower frequency ranges since the slightest changes in the design or in the fabrication, due to processing tolerances can lead to a totally different result than expected. Therefore it is vital to know as much as possible about each single component needed to run the desired application.

To gain information on the components or structures needed to implement a mm-wave RFID transponder, accurate measurements of these networks are required. The theory of characterizing networks at RF to mm-wave frequencies is summarized in Chapter 3.

Chapter 3

Network Measurement Theory

As mentioned before measurements are vital to gain information about a device. Not just that it is also necessary to verify if the device is working within the desired specifications. Furthermore it is used to create a model for a simulation, to compare a simulation with measurements and to adjust parameters for modeling the device behavior.

To successfully perform measurements of different types of electrical networks some fundamental descriptions are necessary, as well as a measurement tool. Detailed information on the connection of the measurement tool to the device under test (DUT) and the DUT itself have to be provided. For this purpose additional calibration measurement are performed. Possible measurement equipment for the characterization of electrical networks are for example a scalar network analyzer or a vector network analyzer (VNA).

3.1   Linear description of Electrical Networks

There are various parameters which describe the linear behavior of an electrical device. These parameters are derived from electromagnetic waves propagating through the device, whereas these waves can be expressed in terms of the voltage between two conductors and the current flowing through the conductors, or as power waves for networks where voltage and current cannot be measured or defined [7]. For a transmission line where the characteristic impedance of the line and the terminating load impedance are not the same (not matched, mismatch), the voltage and current in dependency of z (where z is the distance the wave has traveled), assuming the loss free case, can be calculated as followed [7].

$$V(z) = V^+ e^{-j\beta z} + V^- e^{j\beta z} \tag{3.1}$$

9
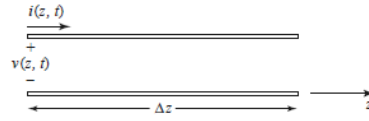
FIGURE 3.1: Transmission Line in dependency of z [3]

$$I(z) = \frac{1}{Z_0}(V^+ e^{-j\beta z} + V^- e^{j\beta z}) \tag{3.2}$$

V^+ is the voltage amplitude of the forward propagating signal, V^- the voltage amplitude of the reflected signal and β is the phase constant (rad/m). Z_0 is the characteristic impedance of the transmission line, only dependent on the geometry and material of the line. The $e^{-j\beta z}$ respectively the $e^{j\beta z}$ terms describe the propagation towards the load (-) or from the load (+) [7]. Defining the reflection coefficient Γ as

$$\Gamma = \frac{V^-}{V^+} \tag{3.3}$$

and the termination impedance Z as

$$Z = \frac{V_0}{I_0} \tag{3.4}$$

the relationship between the reflection coefficient and the termination impedance can be derived as

$$Z = Z_0 \frac{V^+ + V^-}{V^+ - V^-} = Z_0 \frac{1 + \Gamma}{1 - \Gamma} \tag{3.5}$$

$$\Gamma = \frac{Z - Z_0}{Z + Z_0} \tag{3.6}$$

Since it is not always possible to measure the voltage or the current, describing the network with power waves seems the logical solution. These wave amplitudes of the forward and backward propagating signal are defined as a and b (Figure 3.2) where $a = V^+/\sqrt{Z_0}$ and $b = V^-/\sqrt{Z_0}$ (for real-valued Z_0) [7].
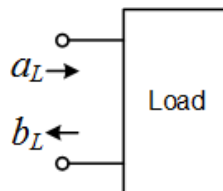
FIGURE 3.2: One-port measurement [4]

The power P is defined as

$$P = \frac{1}{2Z_0}(|V^+|^2 - |V^-|^2) \tag{3.7}$$

If Z_0 is purely real, the power is given by

$$P = \frac{1}{2}(|a|^2 - |b|^2) \tag{3.8}$$

The power of the forward propagating wave is $|a|^2/2$ respectively the power of the backward propagating wave is $|b|^2/2$. Equation 3.8 enables the definition of propagation in terms of wave amplitudes. Furthermore are these amplitudes directly related to the power in the wave. Independent of the type of wave-guide the forward and backward traveling power can be measured unlike voltages and currents. Therefore a parameter model using wave amplitudes is commonly accepted to describe the behavior of a linear electrical network [7].

3.1.1 Scattering Coefficients, S-parameters

The behavior of a linear electrical network is characterized by the S-parameters. Those parameters are utilized in the field of electrical and electronic engineering for design and calculation of microwave systems.

Since the S-parameters do not use open or short circuit conditions to characterize a linear electrical system (in contrast to the Y and Z-parameters), but matched loads, they are more appropriate to measure at higher frequencies. Open and short circuit conditions are hard to realize at high frequencies. Therefore the S-parameter representation is the most important when it comes to measurements. If an other representation is needed the S-parameters can be transformed different two-port parameters, for example Impedance Z, Admittance Y or the so called T-parameters (and others).

The S-parameters describe the correlation between incident and reflected power waves in the electrical system.

Figure 3.3 shows the S-parameter representation for a two-port.

Whereas the incident amplitude waves a_N (N is the number of the port) and the reflected amplitude waves b_N are described as:

$$a_N = \frac{1}{2} \cdot \left(\frac{V_N}{\sqrt{Z_0}} + I_N\sqrt{Z_0}\right) \tag{3.9}$$
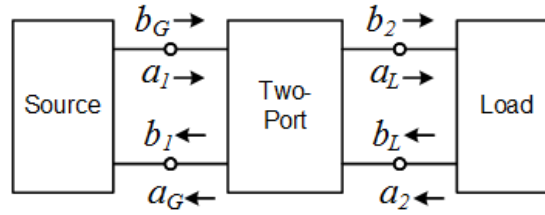
FIGURE 3.3: Two-port representation amplitude waves [4]

$$b_N = \frac{1}{2} \cdot \left(\frac{V_N}{\sqrt{Z_0}} - I_N \sqrt{Z_0} \right) \tag{3.10}$$

Using the relationship between those two waves, the S-parameters are able to express various electrical properties of the device under test, such as gain/insertion loss, voltage standing wave ratio and reflection coefficient.

For a two port network (Figure 3.3) the S-parameters relationship between the reflected and incident waves are as followed:

$$\begin{pmatrix} b_1 \\ b_2 \end{pmatrix} = \begin{pmatrix} S_{11} & S_{12} \\ S_{21} & S_{22} \end{pmatrix} \begin{pmatrix} a_1 \\ a_2 \end{pmatrix} \tag{3.11}$$

Each parameter describes a different characteristic of the electrical network and can be obtained by the following properties if either the first or second port are terminated with a perfect match. This matching condition assures that just one incident wave is entering the system [7].
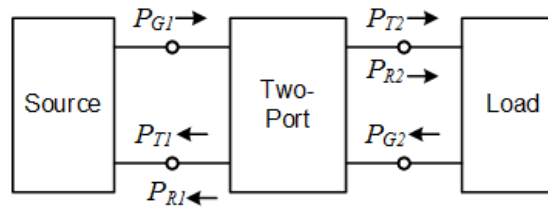
FIGURE 3.4: Two-port measurement power waves [4]

The S_{11} parameter describes of how much of the incident wave a_1 is reflected back to port 1. Therefore it is called the reflection coefficient at port 1 if port 2 is terminated with a matched load. The reflection coefficient gives information about the mismatch of the network without the influence of any other devices that may be connected to port 2.

$$S_{11} = \left.\frac{b_1}{a_1}\right|_{a_2=0}$$

$$S_{11}\big|_{dB} = 20 \cdot log_{10}\frac{b_1}{a_1} = 10 \cdot log_{10}\frac{P_{R1}}{P_{G1}}$$

(3.12)

The S_{21} parameter describes the proportion of the incident wave a_1 which is transmitted to port 2. It is called the transmission coefficient or insertion loss for passive networks.

$$S_{21} = \left.\frac{b_2}{a_1}\right|_{a_2=0}$$

$$S_{21}\big|_{dB} = 20 \cdot log_{10}\frac{b_2}{a_1} = 10 \cdot log_{10}\frac{P_{T2}}{P_{G1}}$$

(3.13)

The S_{12} parameter, similar to S_{21}, describes the proportion of the incident wave a_2 being transmitted to port 1.

$$S_{12} = \left.\frac{b_1}{a_2}\right|_{a_1=0}$$

$$S_{12}\big|_{dB} = 20 \cdot log_{10}\frac{b_1}{a_2} = 10 \cdot log_{10}\frac{P_{T1}}{P_{G2}}$$

(3.14)

The S_{22} parameter, similar to $S11$ describes how much of the incident wave a_2 is reflected back to port 2.

$$S_{22} = \left.\frac{b_2}{a_2}\right|_{a_1=0}$$

$$S_{22}\big|_{dB} = 20 \cdot log_{10}\frac{b_2}{a_2} = 10 \cdot log_{10}\frac{P_{R2}}{P_{G2}}$$

(3.15)

This representation also applies to multi-port devices with more than two ports. The S-parameter matrix grows by one dimension for each port.

For transformation of the S-parameters to any other parameter representation see [8].

3.2 Measurement Tools

Depending on the desired information about the device under test, various measurement tools are available. For measurement of microwave structures the vector network analyzer (VNA) is the most important one. Other important tools for measurements of electrical networks are the scalar network analyzer, combined of a RF tracking generator and a power detector (i.e. spectrum analyzer). Only the VNA will be described since is the only tool able to characterize the DUT in magnitude and phase.

3.2.1 Vector Network Analyzer

The vector network analyzer (VNA) is one of the most important measurement devices to analyze the behavior of an electrical network. Especially since it is applicable for almost any active or passive network.
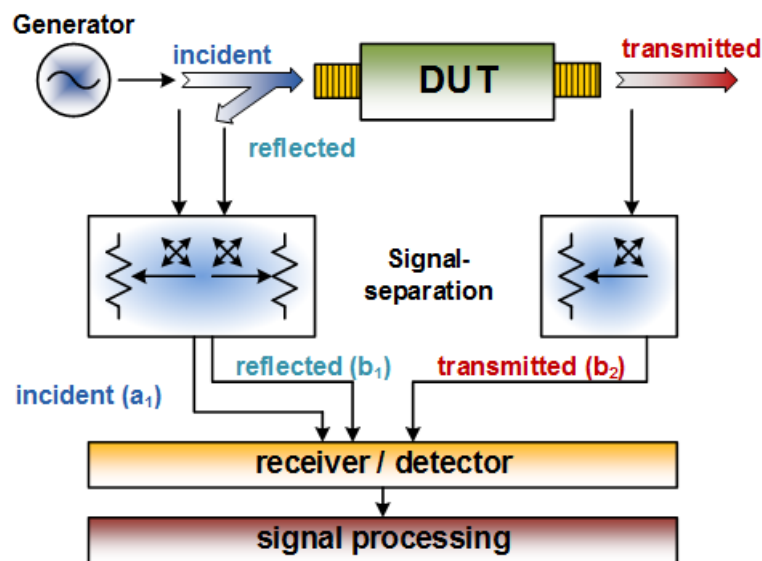
FIGURE 3.5: VNA components [4]

Figure 3.5 shows the principle components of a VNA. It contains the generator, the signal separation, the receiver/detector and the signal processing.

- **Generator**

  The generator provides the excitation signal for the whole system. This signal is variable in frequency as well as in its power level. It has to tune it very quickly and has to have a high frequency stability. Furthermore the frequency resolution also has to be very high to be able to measure narrow band systems. The generator should also have a very linear behavior especially when measuring active devices to avoid harmonics or inter-modulation products [4].

- **Signal-separation**

  For the measurement of the S-parameters the VNA needs both the incident and the reflected signal. The signal-separation provides the signal of the generator for the measurement of the DUT and separates the incident and the reflected signal. For precise measurement the signal-separation should have a high isolation between the incident and the reflected signal and also hardly any insertion loss.
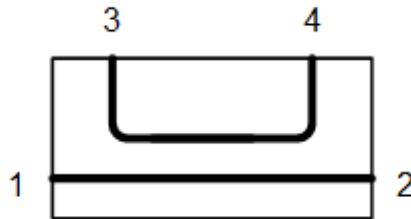
FIGURE 3.6: Directional coupler [4]

Depending on the frequency band various signal-separation units are used. One example is the directional coupler which is a passive device with 4 ports. Depending on the input port the signal is transferred to two other ports. The forth port is decoupled/isolated. The S-matrix of an ideal directional coupler (Figure 3.6) is

$$
S = \begin{pmatrix} 0 & S_{12} & S_{13} & 0 \\ S_{21} & 0 & 0 & S_{24} \\ S_{31} & 0 & 0 & S_{34} \\ 0 & S_{42} & S_{43} & 0 \end{pmatrix}
\tag{3.16}
$$

where the paths port 1 to port 2 and port 3 to port 4 are the so called main paths, and the other paths (port 1 to port 3 and port 2 to port 4) are the coupled paths. An ideal directional coupler would be a perfect solution to separate the incident and reflected signal. However there is no ideal directional coupler. Besides an insertion loss the ports 1 and 4 as well as the ports 2 and 3 are not perfectly decoupled. This unwanted quantity of a directional coupler is considered in the directivity. The directivity describes the ratio $-20 \cdot log_{10}(\frac{S_{41}}{S_{31}})$. To minimize the influence of the directivity either port 3 or port 4 are terminated.
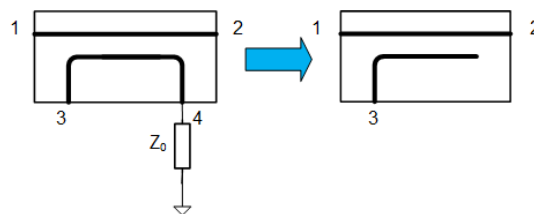
FIGURE 3.7: Directional coupler with terminated port 4 [4]

- **Receiver/Detector**

  A detector uses a local oscillator to mix the high frequency (HF) signal into an intermediate frequency (IF) band where it is filtered by a narrow-band IF-filter (Figure 3.8).
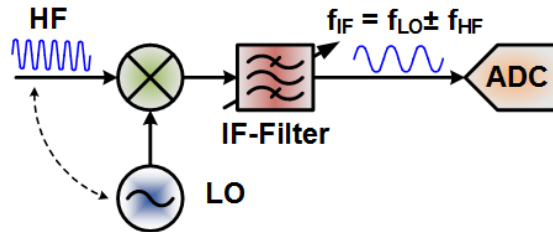
FIGURE 3.8: Mixing and filtering a HF signal [4]

A narrow IF-filter bandwidth increases the sensitivity of the system which also increases the dynamic of the VNA. A higher generator power level as well as averaging have a positive influence on the dynamic range of the system too. The IF-filter furthermore suppresses noise signals such as harmonics of the signal. A high sensitivity or dynamic range does not concur with a fast measurement. Therefore a compromise has to be found between the duration of the measurement and the required sensitivity or frequency resolution.

Figure 3.9 shows the complete block diagram for a two-port VNA. For a two port measurement four signal detector units are necessary to analyses all four power waves a_1, b_1, a_2 and b_2. The local oscillator has to be locked on to the generator to maintain the phase information when mixing the signal to the intermediate frequency range.
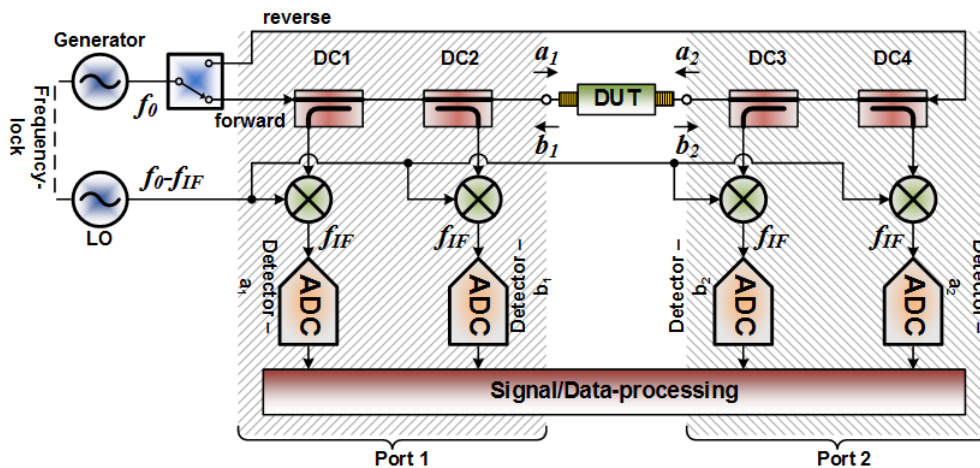
FIGURE 3.9: VNA block diagram [4]

3.3 Calibration

3.3.1 Necessity of Calibration

A real VNA has non ideal components which lead to unavoidable errors. In order to measure the behavior of the device under test (DUT) and not the behavior of the directional coupler, connectors and cables calibration is necessary. Other systematic errors are the generator mismatch, the directivity and the cross-talk. Those errors can be eliminated for the most part by calibration. When calibrating a VNA the reference planes are moved to the desired or available point where the actual measurement should be accomplished. Running a so called calibration routine, enables the VNA to perform an error correction procedure. Thereafter the VNA is calibrated at this point of interest which means that the systematic errors occurring between the DUT and an ideal VNA are corrected.

3.3.2 Error Correction Model

Error correction using calibration can be done for systematic errors since these are the predictable and compensate-able ones. To create a mathematical model, the non ideal VNA is represented as an ideal VNA connected to a two-port network representing the linear systematic error terms of the VNA, the connectors and the cables (Figure 3.10).
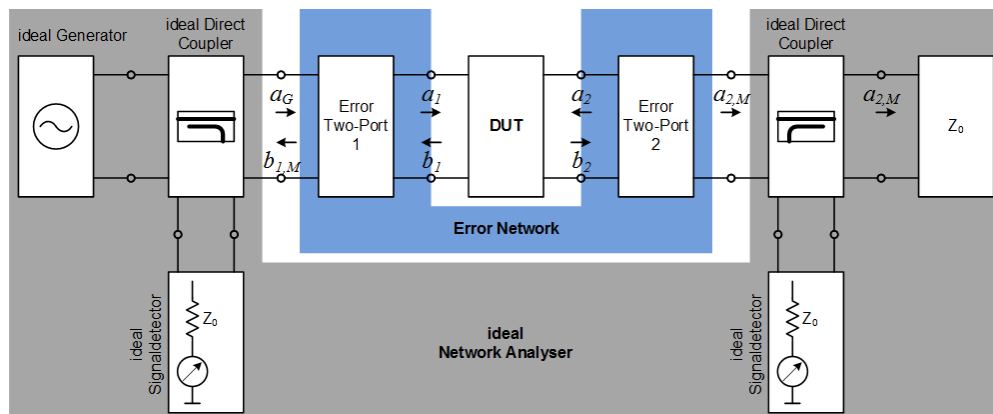
FIGURE 3.10: Model of a vector network analyzer [4]

The complexity of the error two-port depends on the different measurement tasks. For a one-port measurement a complexity of three terms (directivity, tracking and port match) is sufficient. Measuring a two-port network requires more parameters for the error network. A complex error two-port needs 15 parameters. Making some assumptions those can be reduced to 12 or 10 parameters and if the crosstalk is neglected the complexity

can be reduced to 7 parameters. Those parameters are identified measuring known two-ports (calibration elements). The calibration elements have to be consistent over the whole measurement frequency range of interest [4].

- **System Error Model**
  Figures 3.11 and 3.12 show the forward and reverse parts of the 12-term error model.
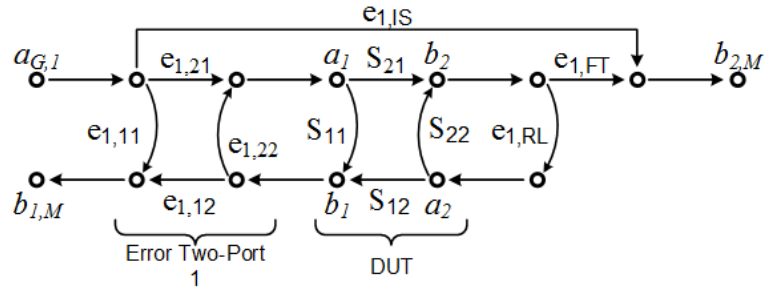
FIGURE 3.11: Forward system error model [4]
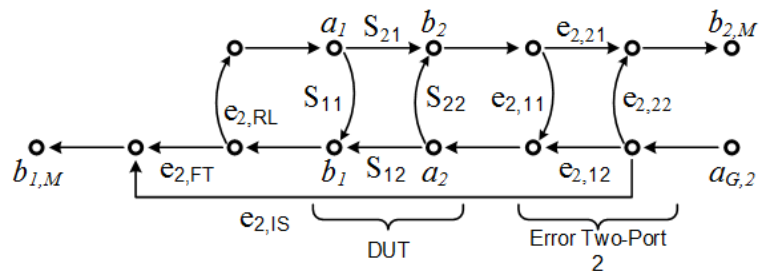
FIGURE 3.12: Reverse system error model [4]

The terms described by this model are [9]:

- **Directivity, $e_{1,11}$**
  The directivity error is increased by cable and connector match errors but caused primarily by the coupler leakage.

- **Reflection Tracking, $e_{1,21}e_{1,12}$ and Transmission Tracking, $e_{1,FT}$**
  Cable length imbalance between the measured ports as well as mixer tracking lead to reflection respectively transmission tracking.

- **Leakage, $e_{1,IS}$**
  The leakage describes the crosstalk between port 1 and 2 and appears through the LO path of the mixers. This model neglects the switch leakage (Figure 3.9).

- **Port 1 Match, $e_{1,22}$ and Port 2 Match, $e_{1,RL}$**
  The match error is the rationed port match error.

Depending on the quality of the calibration standard used, these errors can be greatly reduced by applying a linear calibration procedure.

Noise and linearity errors, however can not be reduced (noise = random error). As well as effects that occur after the calibration of the vector network analyzer (drift errors). Those errors lead to re-calibration of the system after a certain period of time, depending on the system usage, environment and the required accuracy.

3.3.3 Coaxial Calibration Elements

- **Short**

  An ideal short represents a reflection factor Γ of -1 over the whole frequency range. The Γ of a real short depends only on its length offset l (Figure 3.13). To model the short for a VNA in most cases only the electrical length is required.

$$S_{11} = e^{-j4\pi\frac{l}{\lambda}} \tag{3.17}$$
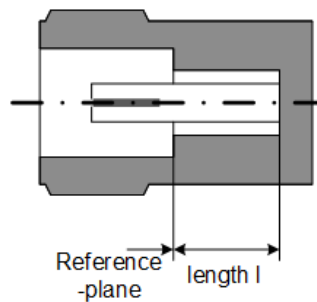
FIGURE 3.13: Short calibration standard [4]

The modeling of parasitic inductances (L_e) is required for precise broadband calibration standards. These parasitic inductances are described as a polynomial of the frequency [5]. Z_L is the characteristic impedance of the coaxial line.

$$L_e(f) = L_0 + L_1 f + L_2 f^2 + L_3 f^3 \tag{3.18}$$

$$S_{11} = \frac{j2\pi f L_e(f) - Z_L}{j2\pi f L_e(f) + Z_L} e^{-j4\pi\frac{l}{\lambda}} \tag{3.19}$$

- **Open**

  The ideal open represents a reflection factor Γ of +1 over the whole frequency range. As the real short a real open is characterized by the offset length l (Figure 3.14) and its parasitic capacitances (C_e) between the inner conductor and the reference ground [5]. Z_L is the characteristic impedance of the coaxial line.
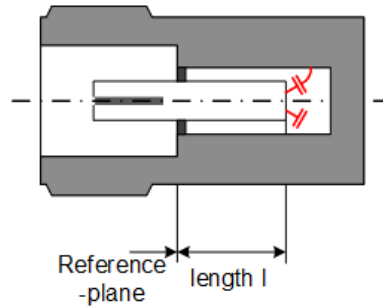
FIGURE 3.14: Open calibration standard [4]

$$C_e(f) = C_0 + C_1 f + C_2 f^2 + C_3 f^3 \tag{3.20}$$

$$S_{11} = \frac{1 - j2\pi f C_e(f) Z_L}{1 + j2\pi f C_e(f) Z_L} e^{-j4\pi \frac{l}{\lambda}} \tag{3.21}$$

- **Match**

  Contrary to the open and short standard a ideal match has a reflection factor Γ of 0. A good real match (Figure 3.15) has a very broad frequency range. Such a behavior can be achieved for coaxial designs where the parasitic capacitances and inductances compensate each other [5].
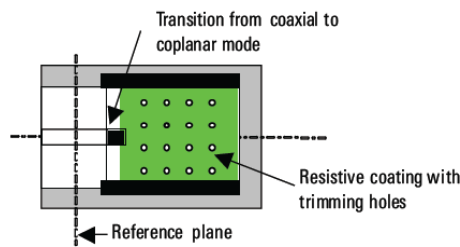
FIGURE 3.15: Match calibration standard [5]

- **Sliding Match**

  The length of the sliding match sets the lower frequency boundary of its use. For frequencies above 8 GHz the sliding match is considered more accurate than a broadband match, due to the precise manufacturing of the used air line sliding match (Figure 3.16) which is more accurate than the one of a match shown in Figure 3.15.

  Figure 3.17 shows the working principle of a sliding match. The reflection coefficient varies with the length offset of the sliding match and lies on a circle if the frequency is constant. The radius of said circle is defined by the return loss of the ferrite cylinder. To determine the characteristic impedance of the air line section, three points on that circle are sufficient [5].
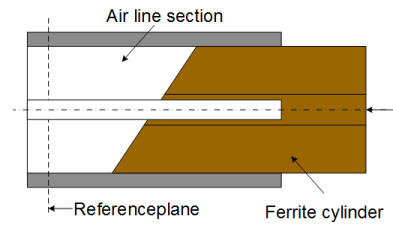
FIGURE 3.16: Sliding Match calibration standard [4]
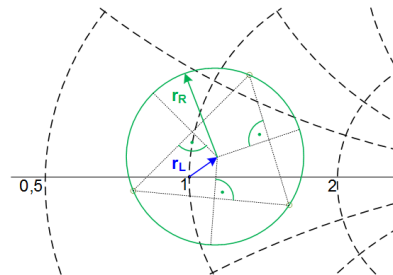
FIGURE 3.17: Determing characteritic impedance [4]

Since measurements are usually performed with frequency sweeps it is not acceptable to measure just three positions of the ferrite cylinder. Changing the frequency results in a movement of the measured points along the circumference but with different speed. To enable a construction of the center these points have to be distributed over the circumference and not be in the same place, which can happen. To avoid this issue more points are measured [5].

- **Through**

  A through connects two test ports directly and in the best case scenario without any delay or insertion loss. Assuming the same connector type is used an ideal trough can only be achieved using a male connector at one port and a female connector at the other. In this case the electrical insertion length is 0. If both connectors have the same gender a small line section is needed to connect these two (Figure 3.18). Thus an insertion loss and an insertion length have to be considered.
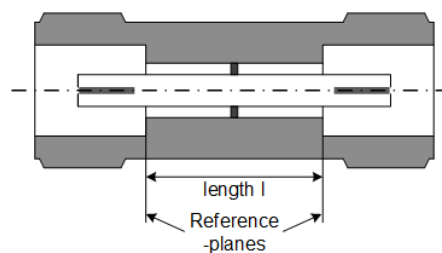
FIGURE 3.18: Through calibration standard [4]

3.3.4 Measurement Errors

There are three different kind of errors occurring when measuring a device.

- **Systematic Errors**

  These errors are time-invariant and occur because of the VNA or the measuring setup. That means that the error is always the same if the setup has not been changed. Therefore they are predictable and correctable. Systematic errors (see Figure 3.19) occurring when working with a VNA are, as mentioned before, the generator/load mismatch, crosstalk, directivity and the connection between the DUT and VNA (connectors and cables) [4].
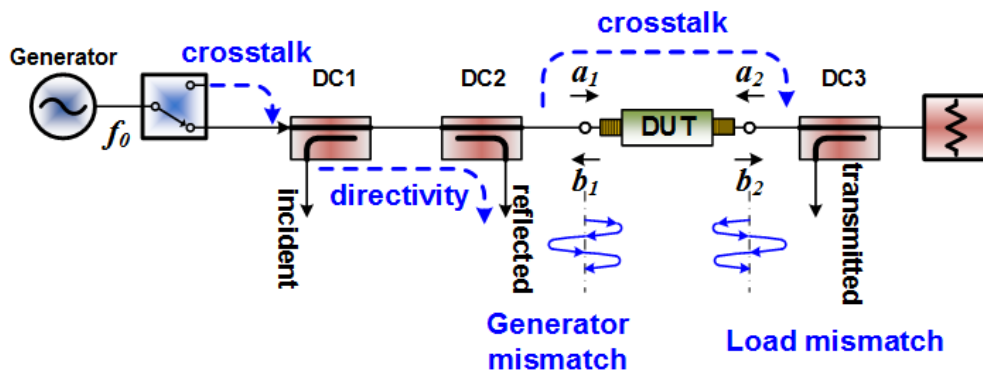
FIGURE 3.19: Systematic errors ocurring in a VNA [4]

- **Random Errors**

  Random errors are not time-invariant and can therefore neither be predicted nor corrected. Main reasons for random errors are the measurement noise and the durability of switches and connectors [4].

- **Drift Errors**

  Errors caused mainly by temperature fluctuations are called drift errors. They appear after the calibration and are also not correctable [4].

3.3.5 One-port Error Model and Calibration

The one-port calibration enables the VNA to analyses the reflection factor of the DUT. Measuring a one-port device the 12-term model is reduced to just three terms. Thus the error network consists of the directivity ($e_{1,11}$), the tracking ($e_{1,21}e_{1,12}$) and the port match ($e_{1,22}$) (Figure 3.20) [9].

The relationship between measured (Γ_M) and actual reflection factor (Γ) is obtained by solving the signal-flow graph shown in Figure 3.20.
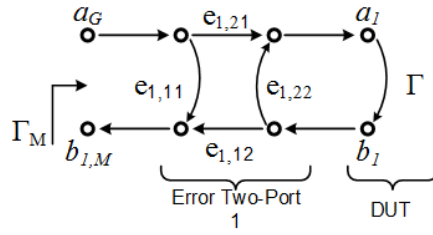
FIGURE 3.20: Signal-flow graph one-port calibration [4]

$$\Delta_e = e_{1,11}e_{1,22} - e_{1,21}e_{1,12} \tag{3.22}$$

$$\Gamma_M = \frac{e_{1,11} - \Delta_e\Gamma}{1 - e_{1,22}\Gamma} \tag{3.23}$$

$$\Gamma = \frac{\Gamma_M - e_{1,11}}{\Gamma_M e_{1,22} - \Delta_e} \tag{3.24}$$

As seen in Equation 3.23 the actual reflection coefficient is modified by the three error terms. Inverting this equation yields the actual reflection factor presumed that the error terms and the measured results are known [9].

Measuring three known standards leads to three equations which determine the error terms. For example measuring the open, short, match/load standards the error parameters can be calculated using the resulting reflection coefficients $\Gamma_{M,L}$, $\Gamma_{M,O}$ and $\Gamma_{M,S}$. Γ_L is the standard for the match/load, Γ_O the standard for the open and Γ_S is the standard for the short. The Γ_L standard is assumed to be perfect for this example. So the tracking term is reduced to e_{21}.

$$\Gamma_{M,L} = e_{1,11} \tag{3.25}$$

$$\Gamma_{M,O} = e_{1,11} + \frac{e_{1,21}\Gamma_O}{1 - e_{1,22}\Gamma_O} \tag{3.26}$$

$$\Gamma_{M,S} = e_{1,11} + \frac{e_{1,21}\Gamma_S}{1 - e_{1,22}\Gamma_S} \tag{3.27}$$

These measurements must be accomplished for the whole frequency range. The resulting parameters are calculated using these equations.

$$e_{1,11} = \Gamma_{M,L} \tag{3.28}$$

$$e_{1,21} = \frac{(\Gamma_O - \Gamma_S)(\Gamma_{M,O} - \Gamma_{M,L})(\Gamma_{M,S} - \Gamma_{M,L})}{\Gamma_S\Gamma_O(\Gamma_{M,O} - \Gamma_{M,S})} \tag{3.29}$$

$$e_{1,22} = \frac{\Gamma_S(\Gamma_{M,O} - \Gamma_{M,L}) - \Gamma_O(\Gamma_{M,S} - \Gamma_{M,L})}{\Gamma_S\Gamma_O(\Gamma_{M,O} - \Gamma_{M,S})} \tag{3.30}$$

The actual reflection coefficient is calculated using the equation 3.24.

3.3.6 Two-port Error Model and Calibration

Using the 12-term error model as shown in Figures 3.11 and 3.12 a two-port calibration is split into the forward and reverse model. The whole measurement setup is presented in Figure 3.10.

Measuring in the forward direction yields to two equations (Equations 3.32 and 3.33) that contain the four actual S-parameters of the DUT as well as the six forward error terms [9].

$$\Delta_S = S_{11}S_{22} - S_{21}S_{12} \tag{3.31}$$

$$S_{11M} = e_{1,11} + (e_{1,21}e_{1,12})\frac{S_{11} - e_{1,RL}\Delta_S}{1 - e_{1,22}S_{11} - e_{1,RL}S_{22} + e_{1,22}e_{1,RL}\Delta_S} \tag{3.32}$$

$$S_{21M} = e_{1,IS} + (e_{1,21}e_{1,FT})\frac{S_{21}}{1 - e_{1,22}S_{11} - e_{1,RL}S_{22} + e_{1,22}e_{1,RL}\Delta_S} \tag{3.33}$$

Another two equations can be found by using the reverse direction.

$$S_{22M} = e_{2,22} + (e_{2,21}e_{2,12})\frac{S_{22} - e_{2,RL}\Delta_S}{1 - e_{2,11}S_{22} - e_{2,RL}S_{11} + e_{2,11}e_{2,RL}\Delta_S} \tag{3.34}$$

$$S_{12M} = e_{2,IS} + (e_{2,12}e_{2,FT})\frac{S_{12}}{1 - e_{2,11}S_{22} - e_{2,RL}S_{11} + e_{2,11}e_{2,RL}\Delta_S} \tag{3.35}$$

Combining the equations for forward and reverse measurement yields four equations which contain all four actual S-parameters and 12 error terms. Provided that the 12 error terms are known (calibration) the actual S-parameters of the DUT can be calculated using these four equations (see for example [9]).

Two calibration methods will be described in this thesis although there are many variants of these two methods [5].

- **SOLT**
  The SOLT method (short, open, load and through) uses the 12-term error model and adds the through measurement to the one-port calibration to turn it into a two-port calibration. It is especially applicable for measurements of coaxial devices.

- **TRL**
  TRL stands for the through, reflect and line method and replaces the load element

of the SOLT method by the characteristic impedance of a line [4]. Depending on the frequency range the reflect element is typically a short or an open. The benefit of this method is that these structures can be manufactured planar structure like on a circuit board (PCB). Important is that the transition from the coaxial connector to the PCB happens always the same way for each calibration element. That enables a characterization of DUTs with non coaxial connectors. The error model simplifies to a 7-term error model (Figure 3.21).
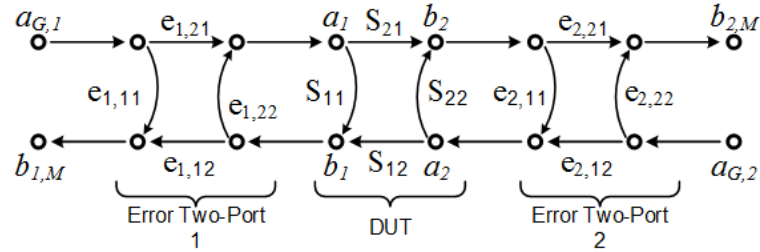

FIGURE 3.21: signal-flow graph two-port calibration 7-term error model [4]

Chapter 4

Calibration-kit up to 3 GHz

The goal of this chapter is to get a deeper understanding on calibration procedures and how calibration kits are designed and fabricated. Ultimately, the knowledge gained by manufacturing an custom calibration kit should help with the design and characterization of the structures at mm-wave frequencies. Since transmission lines and connectors have a huge impact on the behavior of the DUT at very high frequencies, it is crucial to set the reference planes of the calibration directly to the input or the output of the DUT, respectively.

This chapter is a step by step guide to design a calibration-kit up to microwave frequencies. The guidelines for the calibration-kit are, that it has to have coaxial connectors for an easy connection to the VNA and that the reference planes are directly at the DUT to cancel the influence of the feeding line and the connector while analyzing the behavior of the DUT (de-embedding). Therefore a suitable calibration method is chosen and designed on a PCB, and a test-fixture to measure and analyze DUTs with different pad sizes is created. After the design and fabrication sections, the performance of the fabricated calibration-kit is evaluated. The manufactured and not perfect calibration-elements are a short, an open and a match. Compared to perfect calibration elements, the short and open will not have a reflection coefficient S_{11} of $|1|$ or $0\,\mathrm{dB}$, respectively S_{11} for the match will not be zero or $-\infty\,\mathrm{dB}$. Therefore the parameters of the parasitic components (inductance, capacitance and resistor) have to be extracted to increase the accuracy of the calibration-kit. However, the reflection coefficients of the manufactured calibration-elements should be as close as possible to the ideal values. For the match a S_{11} below -25 dB over the whole frequency range provides a sufficient accuracy for this application.

4.1 Considerations

When designing an on-board calibration-kit, various choices have to be made, depending on the set frequency range, the chosen manufacturer and the budget. Another question is, which calibration method is suitable respectively the best fit for the required frequency range. Furthermore it has to be determined, what the characteristic impedance of the calibration-kit should be and which connector fulfills the requirements of a good transition between the feeding cables, coming from the VNA, and the PCBs. The choice of which wave-guide type, for example micro-strip or grounded co-planar wave-guide (GCPW), which are the most commonly used wave-guide types on PCBs, fits best for the desired application has also to be done.

The calibration-kit design discussed in this thesis has a characteristic impedance of $50\,\Omega$. The frequency range is set from DC up to $3\,\text{GHz}$, because the application of the test-fixture is set for frequencies up to $3\,\text{GHz}$. Also the used substrate is not suitable for high microwave frequencies applications, but cheap and it provides an acceptable performance for the set frequency range. The calibration-kit is fabricated by the Institute for Electronics at the Graz University of Technology. The choice of this manufacturer decreases the costs of the PCBs significantly, but it also means that some fabrication limits have to be considered. For example, a circuit board with inner copper layers is not possible, that means the minimal distance between two copper layers is determined by the thickness of the chosen substrate. Furthermore the drill size of the vias is also restricted to be greater or equal to $0.5\,\text{mm}$. The chosen connector is a SMA $50\,\Omega$ End Launch connector (142-0701-806) from Johnson Components. It has four ground pins. Two for the top layer and two for the bottom layer. The vertical distance between those pins determines the substrate thickness, which in this case is $1.5\,\text{mm}$.

The chosen characteristic impedance Z_0, the thickness of the transmission line t, the dielectric constant ϵ_r of the substrate, the frequency range, the substrate thickness h and most importantly the choice of the wave-guide type determine the width W of the transmission line.

4.1.1 Wave-guide Types

The most commonly used wave-guides on PCBs are the so called planar transmission lines, since they are compact, low in cost and can be easily integrated to form an integrated circuit [3]. Typical geometries are strip-lines, micro-strip lines, slot lines, co-planar wave-guides, and other types of related geometries [3].

Out of these geometries the micro-strip line and the grounded co-planar wave-guide are

the most spread, since they are easy to design, to fabricate and easily integrated with active and passive devices [3].

- **Micro-strip Line**

  The micro-strip line geometry is a transmission line with the width W on the top of a substrate with the thickness h and a wide spread ground plane on the bottom of the substrate (Figure 4.1). t denotes the thickness of the metal layer.
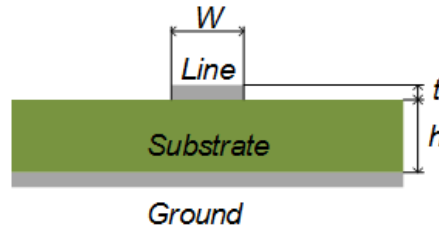

  FIGURE 4.1: Crosssection of a Micro-strip Line

  The characteristic impedance Z_0 of a micro-strip line depends on the ratio of W/h and can be approximated as followed [3].

  $$Z_0 = \begin{cases} \frac{60}{\sqrt{\epsilon_e}} ln \left(\frac{8h}{W} + \frac{W}{4h} \right) & \text{for } W/h \leq 1 \\ \frac{120\pi}{\sqrt{\epsilon_e}[W/h+1.393+0.667ln(W/h+1.444)]} & \text{for } W/h \geq 1 \end{cases} \tag{4.1}$$

  ϵ_e is the effective dielectric constant.

  $$\epsilon_e = \frac{\epsilon_r + 1}{2} + \frac{\epsilon_r - 1}{2} \cdot \frac{1}{\sqrt{1 + 12h/W}} \tag{4.2}$$

  The drawback of micro-strip lines is that they are not shielded and are vulnerable to cross-talk, if another transmission line is in close proximity of the micro-strip line. Also, the mode of the electromagnetic wave changes if, for example a ground plane is too close to the transmission line, which would change the characteristic impedance and the overall behavior of the micro-strip line.

- **Grounded Co-planar Wave-guide (GCPW)**

  The GCPW geometry is similar to the micro-strip line, but it adds a top ground plane, which is connected with vias to the bottom ground (Figure 4.2). That changes the electromagnetic wave mode drastically and the characteristic impedance is now not only determined by the ratio of W/h but also by the size of the gap between the transmission line and the top ground planes.

  The GCPW requires a higher design and fabrication effort, but it also enables a smaller overall design, since the clearance between the wave-guide and another
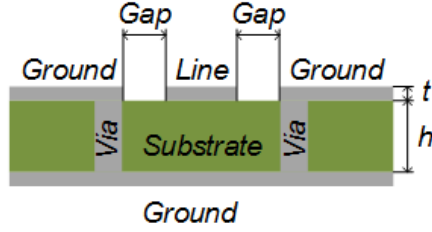
FIGURE 4.2: Crosssection of a Grounded Coplanar Waveguide

electrical structure is determined by the gap size. Increasing the gap size ultimately transforms the GCPW into a micro-strip line.

The characteristic impedance can be found using the following formulas from [10]. Where a is the line width W and b is the sum of W plus the two gap sizes. $K(k)$ is the complete elliptical integral of the first kind and $K(k')$ is the complete elliptical integral of the first kind and complementary modulus [10].

$$Z_0 = \frac{\eta_0}{2 \cdot \sqrt{\epsilon_e}} \cdot \frac{1}{\frac{K(k)}{K(k')} + \frac{K(k_l)}{K(k_{l'})}} \tag{4.3}$$

$$k = a/b \tag{4.4}$$

$$k' = \sqrt{1 - k^2} \tag{4.5}$$

$$k_{l'} = \sqrt{1 - k_l^2} \tag{4.6}$$

$$k_l = \frac{tanh\left(\frac{\pi \cdot a}{4 \cdot h}\right)}{tanh\left(\frac{\pi \cdot b}{4 \cdot h}\right)} \tag{4.7}$$

$$\epsilon_e = \frac{1 + \epsilon_r \cdot \frac{K(k') \cdot K(k_l)}{K(k) \cdot K(k_{l'})}}{1 + \frac{K(k') \cdot K(k_l)}{K(k) \cdot K(k_{l'})}} \tag{4.8}$$

4.2   Idea

Many devices do not have coaxial connectors, but the reference planes of most calibration methods are tailored for coaxial connectors. To be able to measure the device without the connector it has to be de-embedded. For example, the TRL calibration standard is able to move the reference planes to the input/output of the device and is not limited to the coaxial connector. However, for low microwave frequencies the length of the lines, required to perform a TRL calibration, is a drawback of this calibration method.

Another way is to build a SOLT calibration kit on the PCB which then looks like a variant of the TRL standard.

The idea is to characterize the connector and the line to the reference plane and then place the calibration elements "open", "short", "match" and "through" there. The

characterization is needed, since these calibration elements will not not show an ideal behavior, for example due to the line and the connectors.

To be able to characterize the line and the connector, the VNA has to be calibrated using a SOLT two-port calibration. This moves the reference planes to the connectors of the DUT. Measuring a perfect symmetrical line (through element), whose center is the desired place of the new reference planes (where the actual DUT will be), it is possible to extract the parameters for each half of the line individually. Each half consists of a feeding line (half of the line length) and a connector. Furthermore to be able to extract the parameters of the feeding line and the connector, the used line has to be reciprocal [8]. This line will then become an ideal through calibration standard, because the distance of the new reference planes is zero. That means no attenuation or phase delay occur. Figure 4.3 shows the different reference planes and the layout of the used through element.
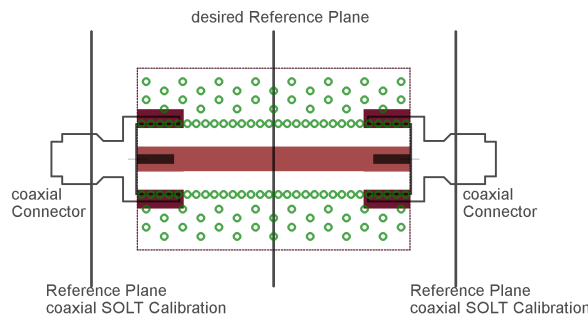

FIGURE 4.3: Through Element with different reference planes

4.3 Design and Realization

The designed circuit boards contain a short, an open, a match, lines with different lengths and structures to measure various electronic components (such as resistors, capacitances and inductances) with different pad sizes (0402,0603 and 0804). One line is twice as long as the feeding line (30 mm). That means this line can be used as the through standard, assuming perfect symmetry and that it is reciprocal. The short, open and match are placed at the end of the feeding line (15 mm). This arrangement enables a SOLT calibration at the end of the feeding line. A SOLT calibration-kit was chosen because for frequencies up to 3 GHz the fabrication of the match with lumped components is still possible assuming that the used resistors are still applicable in this frequency range and because a TRL calibration-kit would need rather long transmission lines to perform a calibration for low frequencies.

The length of the feeding line was chosen to be 15 mm for an easier handling of the circuit boards.

The circuit boards are fabricated by the Institute for Electronics at the Technical University of Graz. All circuit boards consist of a substrate and two copper layers on top and at the bottom of the substrate, which makes them two-layer circuit boards. Such a board is easier and cheaper to fabricate than PCBs with layers within the substrate (for example a four layer board would have a top copper layer, a substrate layer, the first inner copper layer, the core substrate, the second inner copper layer, another substrate and the bottom copper layer). The substrate thickness is 1.5 mm and is preconditioned by the size of the SMA connectors.

The desired type of wave-guide would be a micro-strip line, because it is easier to design and fabricate than a grounded GCPW. For the given parameters the width of the micro-strip line can be calculated to 2.8 mm and a minimum clearance of 9 mm which is not given because the SMA connectors do not provide this clearance. That is why a GCPW (see Figure 4.2) design is used. The line width is 2.7 mm and the clearance/gap is 2.05 mm. This results of the maximal available space in between the SMA connector, and the substrate thickness.

When using a GCPW it is vital that the neighboring ground planes to the transmission line have an almost perfect connection to the bottom ground plane, because the GCPW is specified for this case only. A change of the mode, which can happen if there is no connection between the top and bottom ground planes would result in a change of the characteristic impedance of the line. To establish this connection, vias are placed as close as possible to each other at the edge of the top ground planes. The size of the vias is preferably the smallest possible (depends on the manufacturer).

The placing of the vias helps in general to avoid undesired standing waves on the ground planes. The distance between two vias should be smaller than the shortest wave length of the highest used frequency.

Figure 4.4 shows the layout and Figure 4.5 the circuit board of the short, match and open calibration elements whose reference planes are moved 15 mm away from the connector. The layout of the through is shown in Figure 4.3. The length of the circuit board is 30 mm.

The short is fabricated by placing vias at the end of the feeding line (Figures 4.4 and 4.5). The length of the via equals the substrate thickness and leads to the parasitic inductances mentioned in 3.3.3. Furthermore the vias are placed in a way, that the inner circumference of the restring is exactly at the reference plane, because that is where the ideal short should be. Placing the via further away, so that the outer circumference of the restring is at the reference plane would increase the parasitic inductances, since the connection to the ground plane is now longer than before.
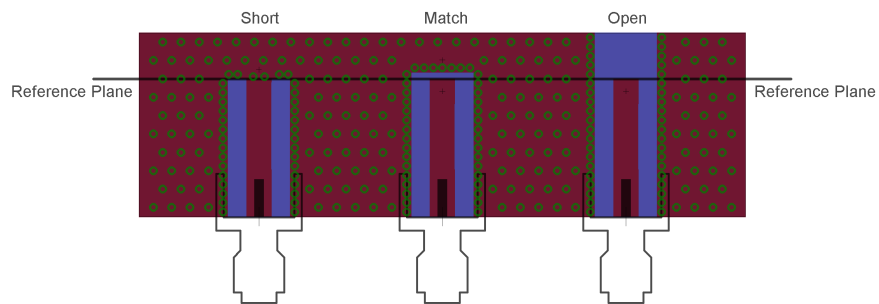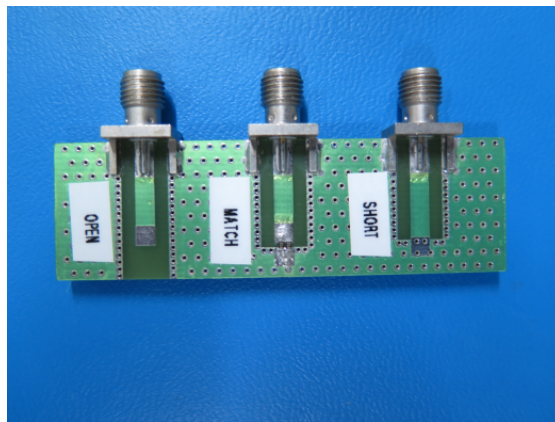
FIGURE 4.4: Short, Open and Match Elements

FIGURE 4.5: Circuit Board for Short, Open and Match

For the open the feeding line ends at the reference plane. To minimize the parasitic capacitances the top ground plane is cut into two separate top ground planes (Figures 4.4 and 4.5).

Since the characteristic impedance of the line is chosen to be $50\,\Omega$, two $100\,\Omega$ resistors are soldered in a parallel manner on the circuit board at the reference plane in order to create a match, because a $50\,\Omega$ resistor is not part of the E24 or E48 series. Furthermore using two $100\,\Omega$ resistors parallel reduces the tolerance of the real component by the factor of two (Figures 4.4 and 4.5).

A test fixture to characterize a device with 0603 pads is shown in Figure 4.6 as a layout and in Figure 4.7 as a circuit board. For this case the reference planes are at the beginning of the 0603 pads. If a device with different pad sizes is to be characterized, the fixture has to be modified respectively the pads have to be adapted to the wanted size.
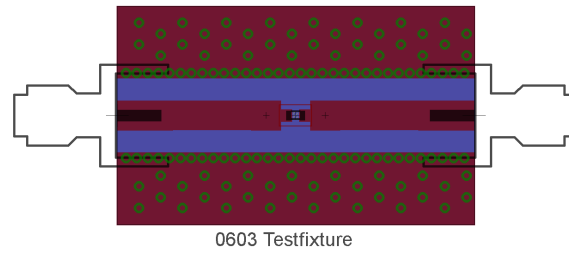
0603 Testfixture

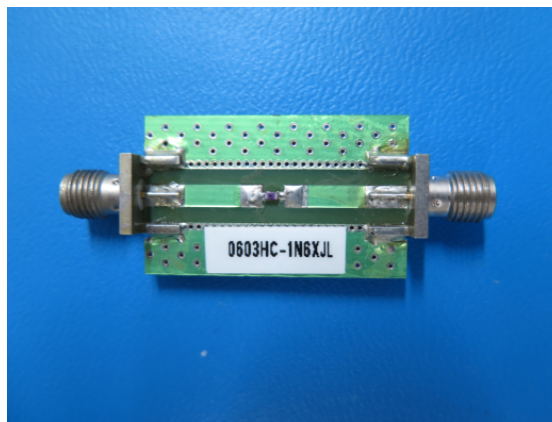FIGURE 4.6: Fixture to measure a 0603 Device

FIGURE 4.7: Coil Circuit Board

The realized through is shown in Figure 4.8. Furthermore a test fixture to analyse the behaviour of different line lengths is shown in Figure 4.9.
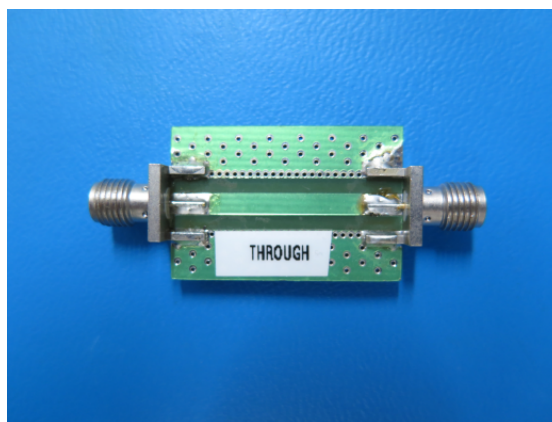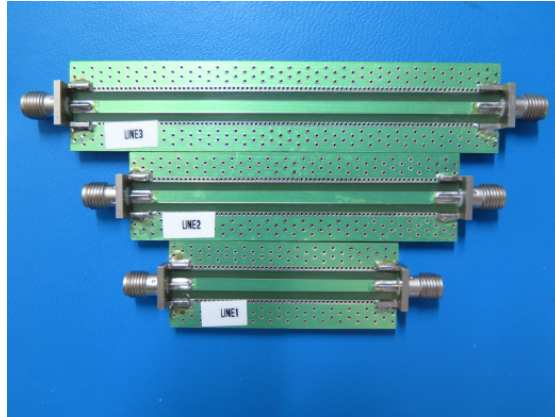

FIGURE 4.8: Through Circuit Board

FIGURE 4.9: Lines Circuit Board

4.4   De-embedding

De-embedding means to be able to analyze a device without any influences of feeding
lines or connectors. As mentioned before, that is possible if the parameters of the
feeding lines and the connectors are known and that the measured through is perfectly
symmetrical and reciprocal. Measuring the through (Figure 4.8) with a calibrated VNA
yields to the S-parameters for this device. Given that the reference plane is exactly
in the middle of the fixture and that it is reciprocal, the parameters of each half can
be calculated using the T-parameters. The S-parameters have not been designed for
calculating series connection of different elements. In this case the fixture is seen as a
series connection of two two-port networks. Using the T-parameters, which assign the
incident and reflected waves differently. Compared to Equation 3.11 the T-parameters
are defined as followed:

$$\begin{pmatrix} a_1 \\ b_1 \end{pmatrix} = \begin{pmatrix} T_{11} & T_{12} \\ T_{21} & T_{22} \end{pmatrix} \begin{pmatrix} b_2 \\ a_2 \end{pmatrix} \tag{4.9}$$

For the transformation of the S-parameters to the T-parameters see [8].

Splitting the electrical network into two two-port networks enables the calculation of
the T-parameters of the feeding line and the connector by taking the square root of the
T-parameters (Figure 4.10).

In order to get the S-parameters of the feeding line, the T-parameters of one half have
to be re-transformed to the S-parameters.

The problem of taking the square root of a complex parameter is the sign change of the
phase that happens at 180°. In Matlab 181° are actually seen as −179°. Which means
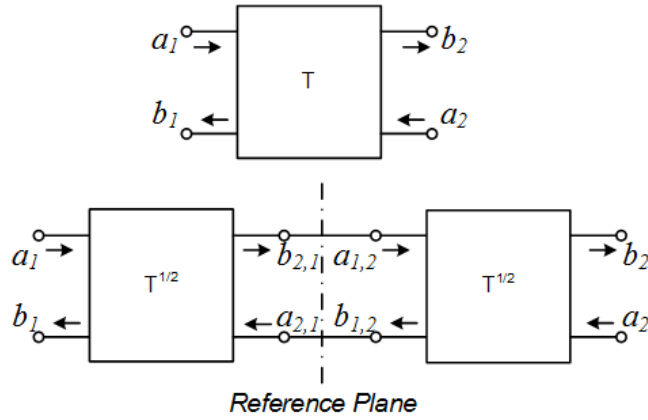that instead of a continuous slope the phase jumps by 180° when taking the square root

FIGURE 4.10: Virtual separation of the Through Element using their T-Parameters

although the real phase change is just, for example 1°.

Example 4.10 shows the problematic happening in Matlab.

$$
\begin{aligned}
c = a \cdot e^{j\varphi} &\rightarrow \sqrt{c} = \sqrt{a} \cdot e^{j\frac{\varphi}{2}} \\
\varphi_1 = 179.5 \qquad & \qquad \varphi_2 = 180.5 \\
\Delta_\varphi = \varphi_2 - \varphi_1 = 1 &\rightarrow \frac{\Delta_\varphi}{2} = 0.5 \\
\frac{\varphi_1}{2} = \frac{179.5}{2} &= 89.75 \\
\frac{\varphi_2}{2} = \frac{180.5}{2} &= \frac{-179.5}{2} = -89.75 \\
\rightarrow \Delta = \frac{\Delta_\varphi}{2} &= 179.5
\end{aligned}
\tag{4.10}
$$

To avoid this problem the linear phase has to be compensated while performing the square root calculation. This is done by estimating the mean time delay (Δ_τ) of the test fixture and subtracting that from the phase of the transmission parameters. That yields a phase shift of 0° in the noise free case. After taking the square root, half of the mean time delay has to be added again to the fixture parameters to regain the phase information.

Example 4.11 shows the phase delay compensation as it is performed in Matlab. φ is the phase of the transmission parameters of the test-fixture (through), φ_{comp1} and φ_{comp2} are the compensated phases, S_{Para} are the S-parameters of the through, $S_{Fixture}$ are the S-parameters of the feeding line and f is the frequency. Note that the phase compensation has only to be done for the transmission parameters S_{21} and S_{12}, because these parameters describe the influence of the system on a wave traveling through it, while the matching parameters S_{11} and S_{22} describe the input, respectively the output impedance of the system.

$$\varphi_{comp1} = angle(e^{j \cdot (\varphi + 2\pi \cdot f \cdot \Delta_\tau)})$$

$$S_{Para} = |S_{Para}| \cdot e^{j \cdot \varphi_{comp1}}$$

$$S_{Para} \rightarrow T_{Para}$$

$$T_{Fixture} = \sqrt{T_{Para}} \qquad (4.11)$$

$$T_{Fixture} \rightarrow S_{Fixture}$$

$$\varphi_{comp2} = angle(e^{j \cdot (\varphi - 2\pi \cdot f \cdot \frac{\Delta_\tau}{2})})$$

$$S_{Fixture} = |S_{Fixture}| \cdot e^{j \cdot \varphi_{comp2}}$$

Knowing the S-parameters of the feeding line the de-embedding for a one-port network can be done using Equation 3.24. Γ_M is the measured reflection coefficient and the error terms are replaced by the S-parameters of the feeding line (Figure 4.11).
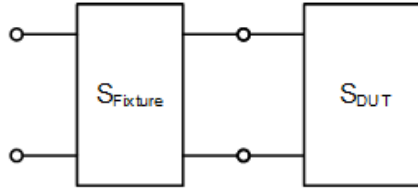

FIGURE 4.11: One-Port Network de-embedding

The de-embedding of a two-port network according to [8] is done as shown in Example 4.12. $S_{Network}$ are the S-parameters of the measured two-port network containing the feeding lines whose S-parameters are $S_{Fixture}$ and S_{DUT} are the desired S-parameters of the DUT (Figure 4.12).
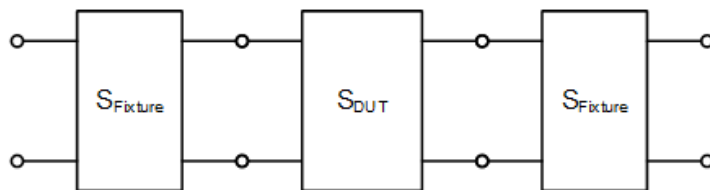

FIGURE 4.12: Two-Port Network de-embedding

$$S_{Network} \rightarrow T_{Network}$$

$$S_{Fixture} \rightarrow T_{Fixture}$$

$$T_{Network} = T_{Fixture} \cdot T_{DUT} \cdot T_{Fixture} \qquad (4.12)$$

$$T_{DUT} = T_{Fixture}^{-1} \cdot T_{Network} \cdot T_{Fixture}^{-1}$$

$$T_{DUT} \rightarrow S_{DUT}$$

4.5 Results

The results are obtained by measuring the various circuit boards with a Rhode & Schwarz ZVL (VNA) which is calibrated using the SOLT calibration-kit from Hewlett Packard 85052B. This means that the reference planes are at the beginning of the feeding lines (Figure 4.3). Therefore the de-embedding, as described before, has to be done. In section 4.5.1 a comparison between the measured and de-embedded results are given. In the following section 4.5.3 the difference between the de-embedded measurements and the measurements being done after calibrating the ZVL with the custom-built SOLT calibration-kit on the circuit boards is shown.

4.5.1 Measurement Results with and without De-embedding

- **Through/De-embedding Fixture**
  The ideal through is used as the de-embedding fixture. It is assumed to be a perfect through at the reference plane. Therefore the insertion loss and phase delay are zero. Performing a de-embedding procedure described in Chapter 4.4, the de-embedding fixture can be calculated from the S-parameters of the realized through (Figure 4.8), by assuming it to be perfectly symmetrical and splitting it virtually into two halves.
  The Figures 4.13, 4.14 and 4.15 show the S-parameters of the through on the left and the S-parameters of the de-embedding fixture calculated on the right. $\tau_{measured}$ and $\tau_{de-embeddingFixture}$ are the estimated group delays. Note that for the de-embedding fixture the group delay should be exactly half of the group delay of the through, which is the case.

  The input/output matching (Figures 4.13) show the match of the through which is below -30 dB.

  The insertion loss is shown in Figure 4.14. In a noise free scenario this figure would show a straight line indicating the attenuation of the through respectively the de-embedding fixture. The higher noise level around 2 GHz could appear because of measurement errors and numerical problems with the phase noise. These errors are not correctable and because the through measurement is used to calculate the de-embedding fixture, they will appear in the following measurements.

  Figure 4.15 shows the group delay of the through and the de-embedding fixture. Due to the de-embedding procedure the group delay of the through is divided in half. Furthermore the measurement errors around 2 GHz are again visible and result in a higher noise level.
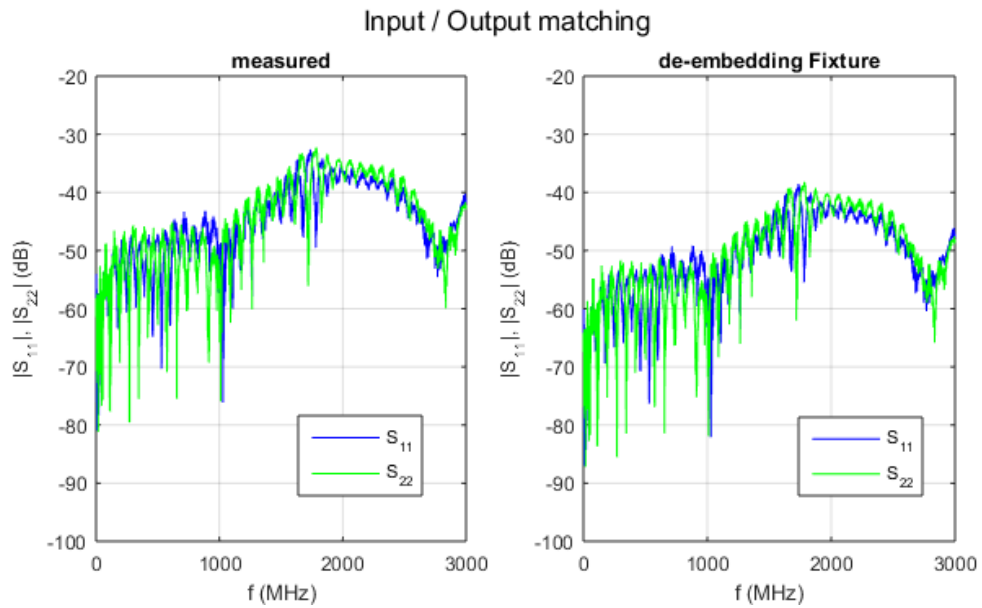
FIGURE 4.13: Input/Output matching of the Through
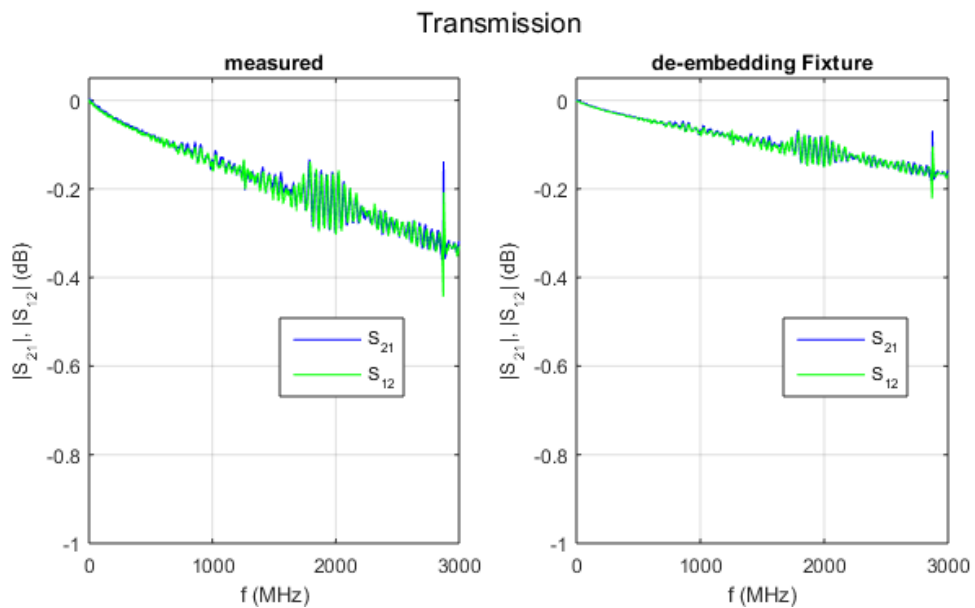

FIGURE 4.14: Transmission of the Through

- **Short**

  As mentioned before, the short is part of the SOLT calibration kit. The Figures 4.16 and 4.17 show the S_{11} of the short. Since it is a one-port network just one parameter can be measured, respectively is needed.

  Figure 4.16 presents the S_{11} before and after de-embedding. While the measurement still shows the effect of the feeding line, the de-embedding is able to compensate it almost completely.
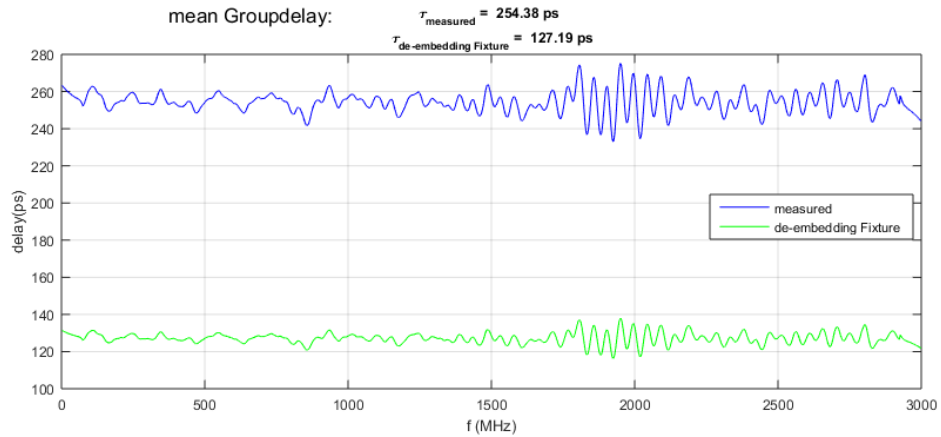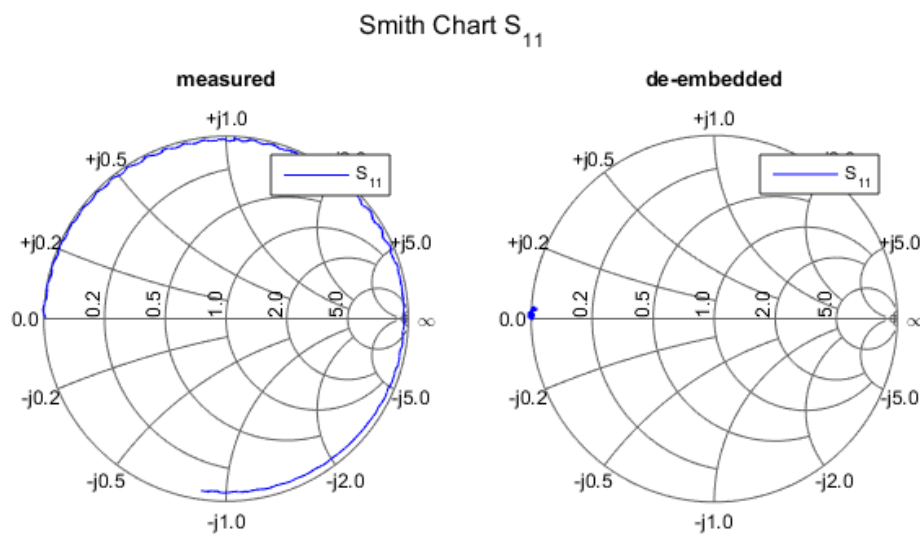
FIGURE 4.15: Groupdelay of the measured Through and the De-embedding Fixture

FIGURE 4.16: Smith-Chart S_{11} of the Short

A perfect short should exhibit a straight line at zero for the S_{11} parameter. That is not the case for any real short, because of the not perfect connection between the transmission line and ground (vias). Figure 4.17 shows the effects of noise, measurement errors and a not perfectly constructed short. The S_{11} of the de-embedded short should never be positive, but since the calculation of the de-embedding fixture is performed using the measurement of the through with all the measurement errors, the de-embedding itself is not perfect.

- **Open**

  Another part of the calibration-kit is the open. Same as for the short, the Figure 4.18 shows the de-embedding respectively the compensation of the feeding line.
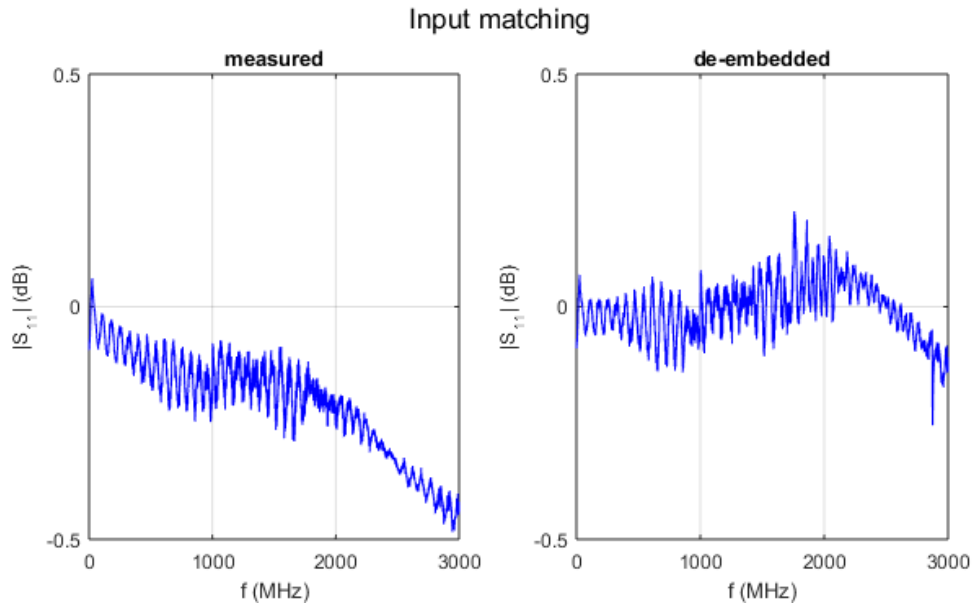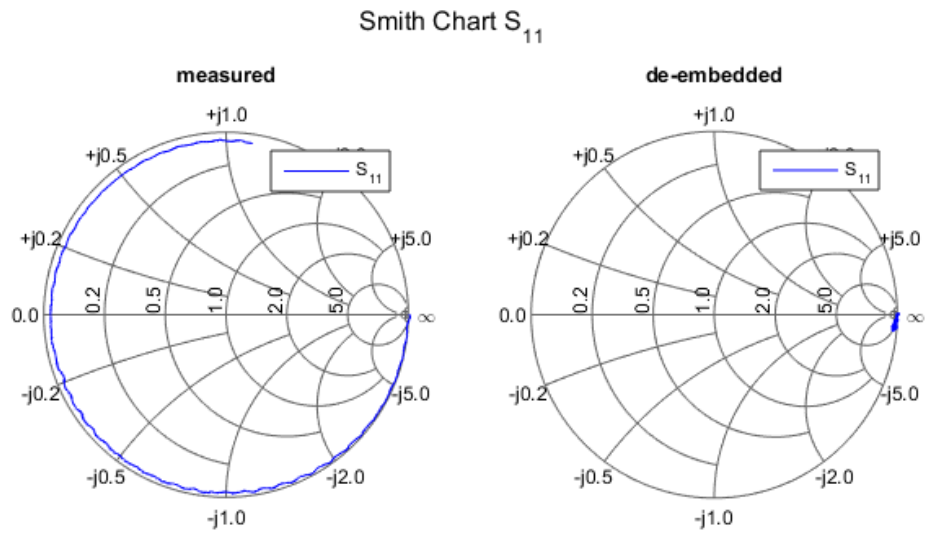
FIGURE 4.17: Input matching of the Short

FIGURE 4.18: Smith-Chart S_{11} of the Open

Figure 4.19 represents the S_{11} parameter of the open. A perfect open would reflect every signal back to its source with a reflection coefficient of $|1|$. That is the case after the de-embedding, except for the noise, measurement errors, parasitic capacitances and the de-embedding process itself which is not perfect.

- **Match**

  The match is the last part of the SOLT calibration-kit. A perfect match does not reflect anything back to the source. After the de-embedding the manufactured
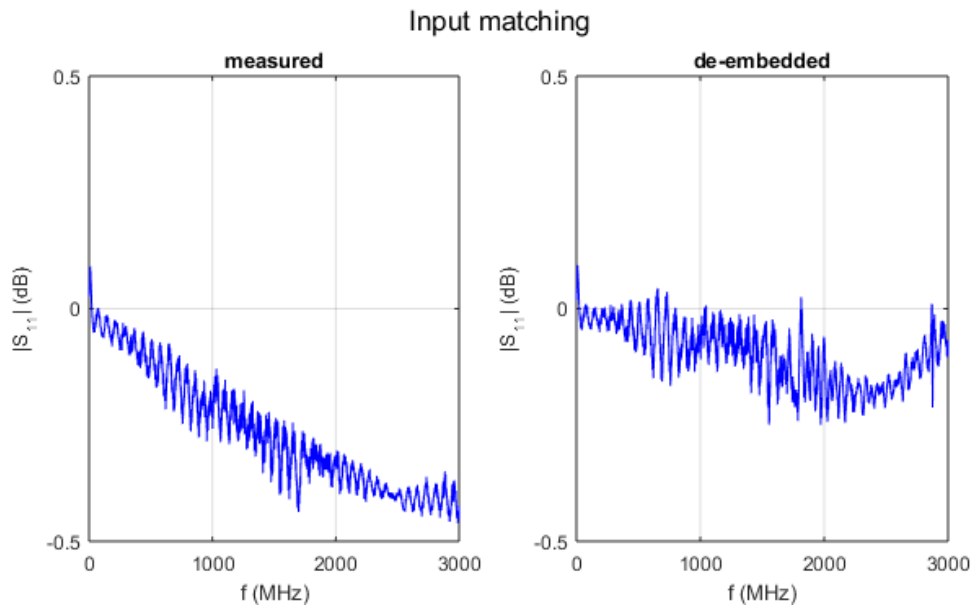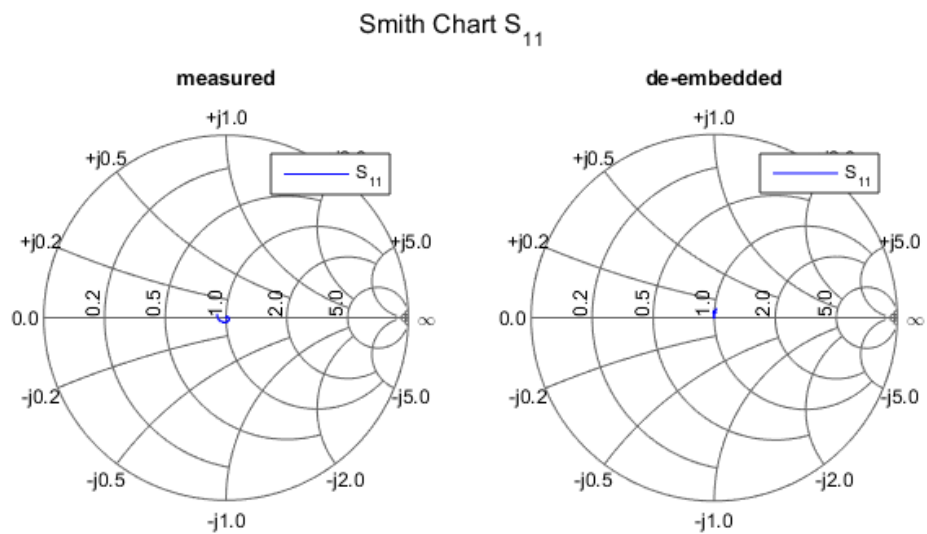
Input matching

FIGURE 4.19: Input matching of the Open

match shows a matching below -27 dB which is acceptable at 3 GHz (see Figures 4.20 and 4.21).

Smith Chart S_{11}

FIGURE 4.20: Smith-Chart S_{11} of the Match

- **Lines**

  The measured lines are used as a comparison between the measurement when the VNA is calibrated with the manufacturers calibration-kit and when it is calibrated with the embedded board calibration-kit.
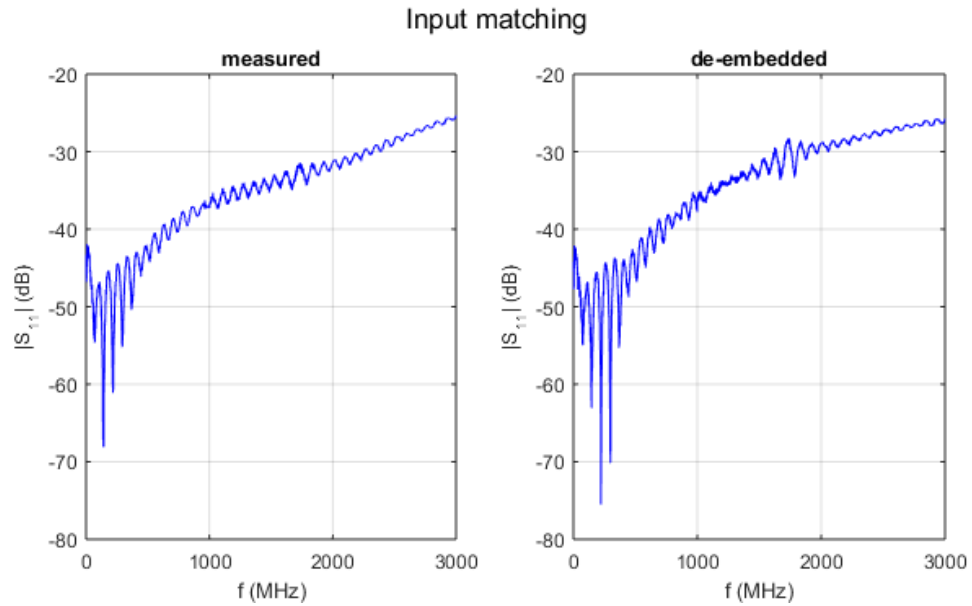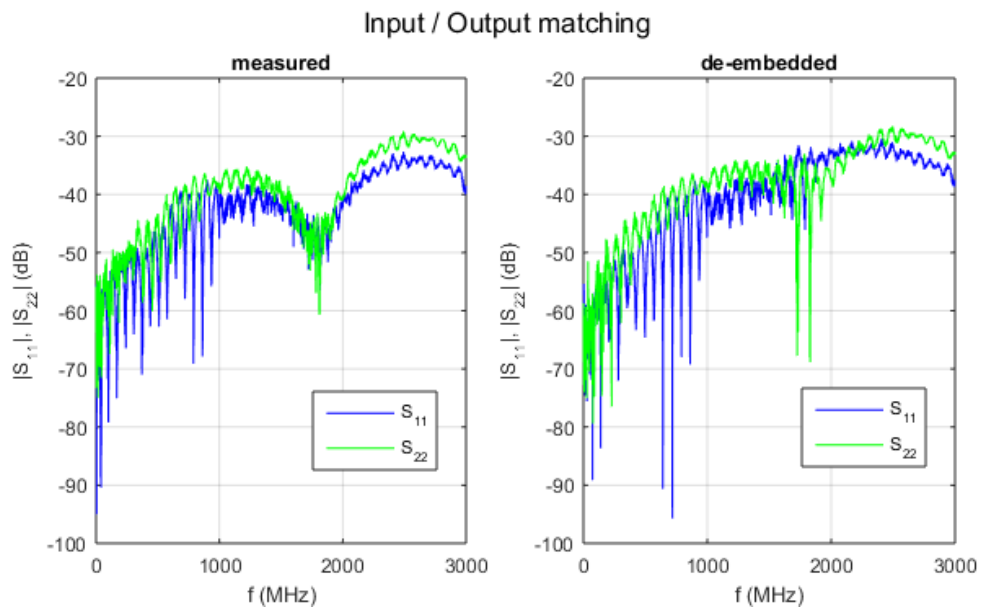
FIGURE 4.21: Input matching of the Match

FIGURE 4.22: Input/Output matching of the Line 1

The matching of the lines 1,2 and 3 before and after de-embedding are shown in Figures 4.22, 4.23 and 4.24. The smith-chart is not very significant for the measurements of the lines. That is why they are not displayed. The insertion loss of a transmission line increases the longer the line is. Due to a not perfect matching at the end of the transmission line, a part of the signal is reflected back to the exciting port, which affects the matching. Therefore will a longer transmission line also result in a better matching because less of the exciting signal is reflected back to the port.
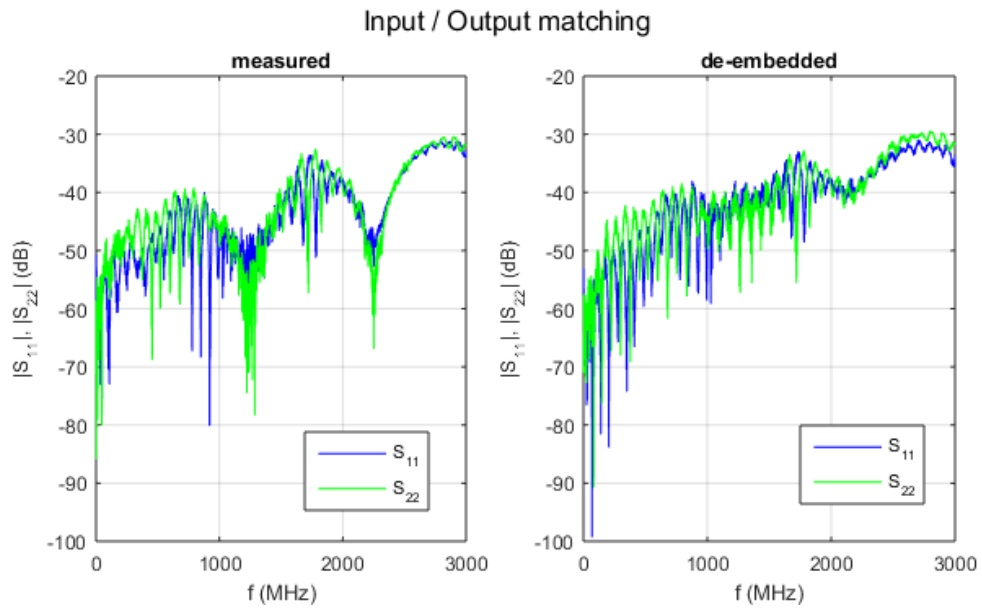
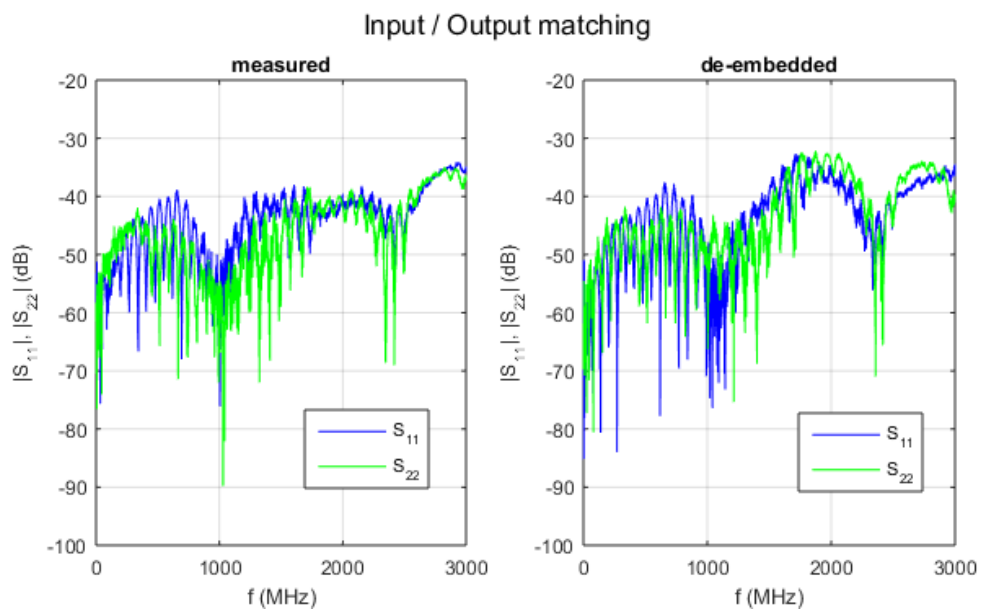FIGURE 4.23: Input/Output matching of the Line 2

FIGURE 4.24: Input/Output matching of the Line 3

The higher noise level around 2 GHz is the same as for the through. The only difference between the three lines is the length. Therefore the insertion loss is higher for line 3 than it is for lines 1 and 2 (Figure 4.25, 4.26 and 4.27).

Line 1 is 22 mm longer than the through. Hence the mean group delay τ_{Line1} after the de-embedding is not 0 ps (mean group delay of the through $\tau_{Through}$) but 129.76 ps. Since line 2 is twice and line 3 three times as long as line 1 the mean group delays τ_{Line2} and τ_{Line3} are twice, respectively three times as big as τ_{Line1} (Figure 4.28). Again the measurement errors around 2 GHz are visible
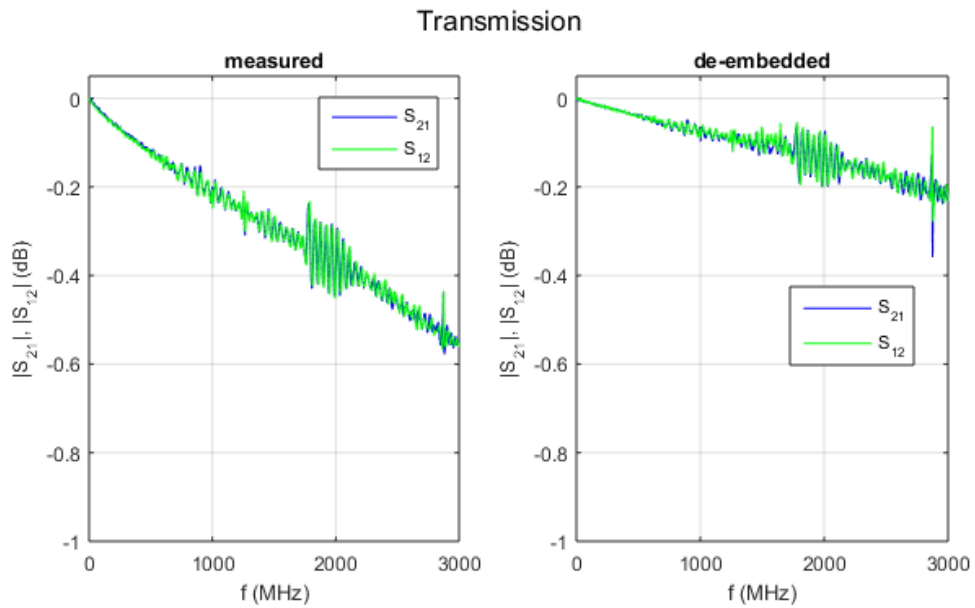
FIGURE 4.25: Transmission of the Line 1
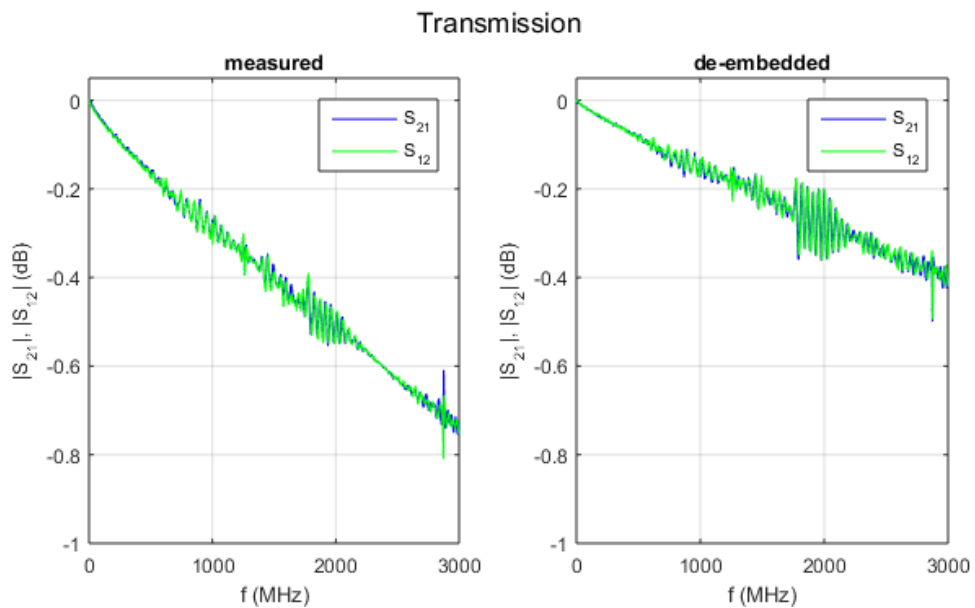
FIGURE 4.26: Transmission of the Line 2

- **Coil**

  The coil 0603HC-1N6XJL is also used as a comparison tool between the manufactured and the circuit board calibration-kit. The results are represented in Figures 4.29, 4.30, 4.31 and 4.32.

  The smith-chart of the coil (Figure 4.32) indicates a typical behaviour of a coil when performing a frequency sweep. Before the de-embedding the affect of the feeding line onto the coil is visible. Due to the fact, that the coil is not ideal but has parasitic resistors, losses occur which can be seen in Figure 4.29. An ideal coil
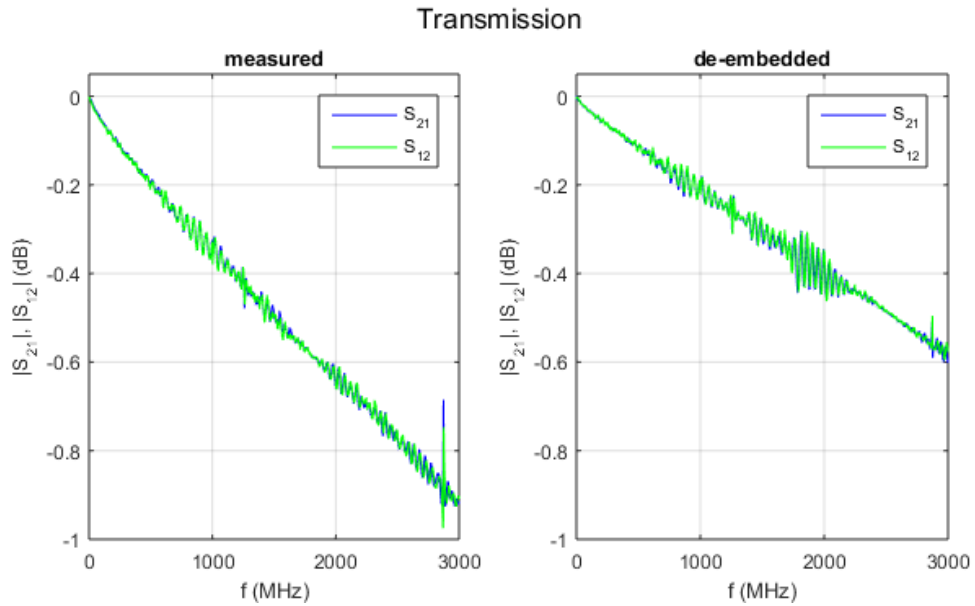
FIGURE 4.27: Transmission of the Line 3
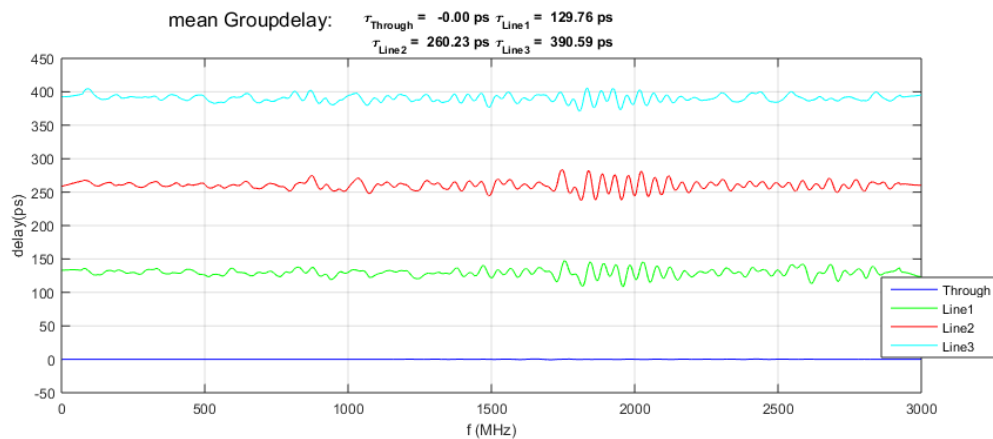
FIGURE 4.28: Mean group delays of the perfect through and the lines 1,2 and 3

would only change its imaginary part of the impedance over the frequency. The slight bend of the curve in Figure 4.29 indicates the losses.

4.5.2 Calibration-kit Parametrization

When calibrating the VNA with the new calibration-kit the values of the kits parameters have to be extracted from the short, open, match and through measurements to increase the accuracy of the measurements being done after the calibration. The idea is to give the VNA as much information as possible about the device being used as a calibration standard to increase the performance of the error reduction.

The VNA allows a maximum degree of the parasitic inductances/capacitances polynomial of three to describe the short, open and match standard. Figure 4.33 shows the
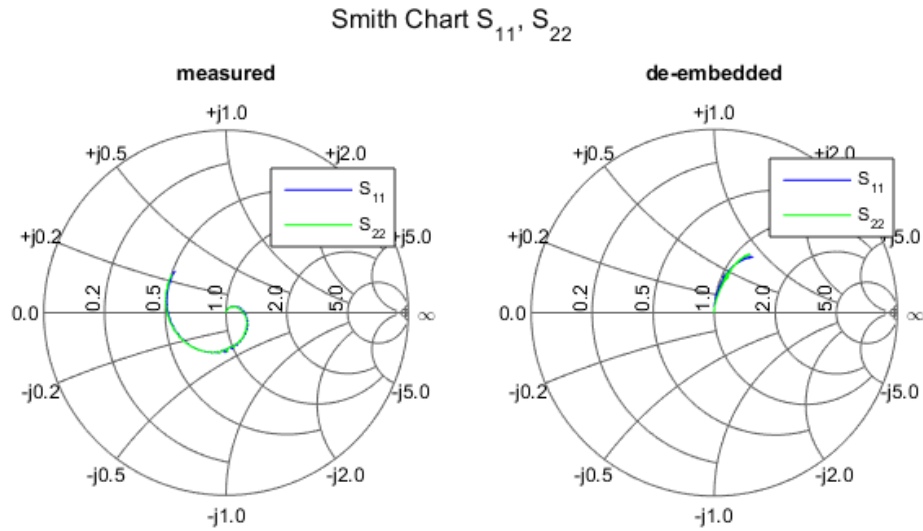
Smith Chart S_{11}, S_{22}

FIGURE 4.29: Smith-Chart S_{11} S_{22} of the Coil

Input / Output matching
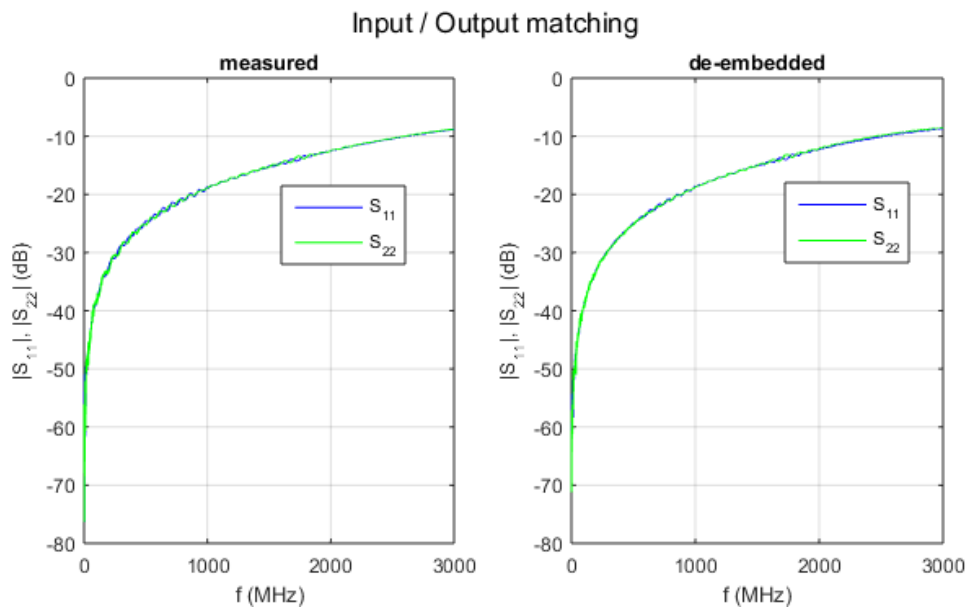
FIGURE 4.30: Input/Output matching of the Coil

elements describing the different standards (open, short, match) for the VNA. The R' ,C ' and L' represent the parasitic effects describing these standards. These parameters are extracted from the de-embedded measurement. For the custom calibration-kit the delay parameter is assumed to be zero as well as the G' parameter, because the parameters are extracted at the desired reference planes (de-embedded) and there is no additional transmission line between the end of the feeding line and the reference planes.

- **Calculation of Short Parameters**

FIGURE 4.31: Transmission of the Coil

FIGURE 4.32: Phase of the Coil
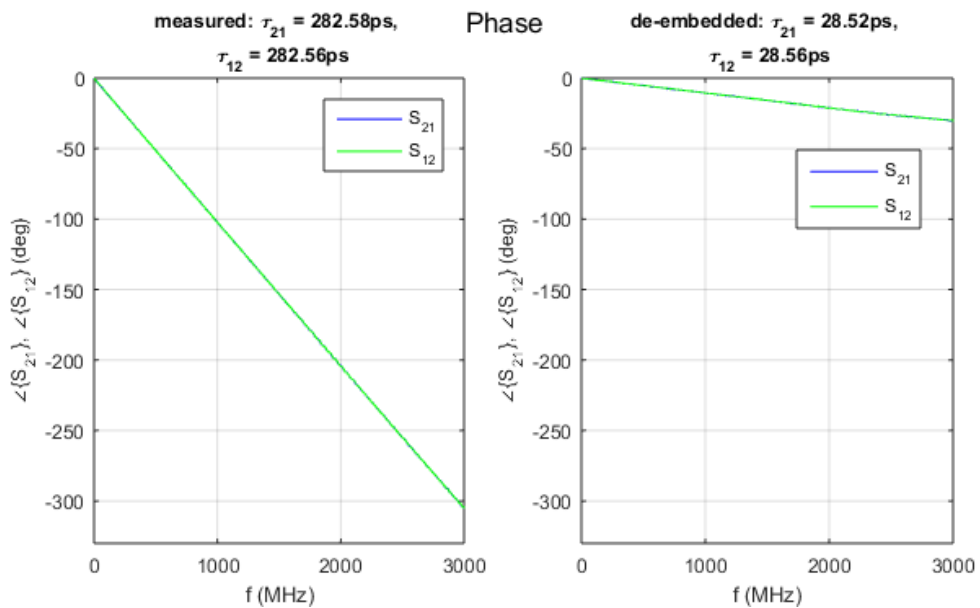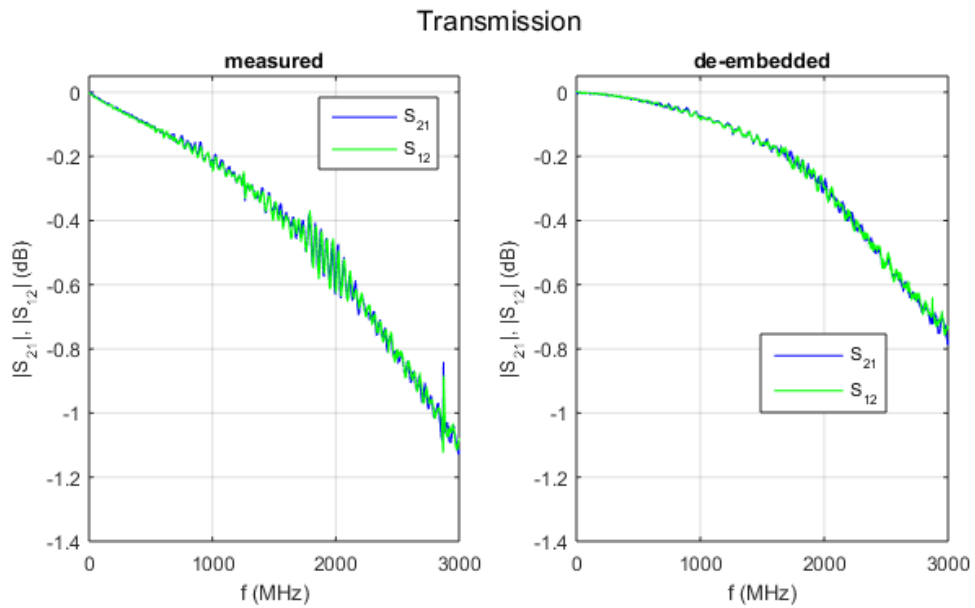
The values of the short parameters are extracted by transforming the S-parameters of the de-embedded short measurement into the Z-parameters, because the parasitic inductances are connected in series to the ideal short, and fitting a polynomial for the parasitic inductances (Figure 4.34) to the resulting curve over the frequency. The accuracy of the curve fitting depends on the order of the polynomial. The coefficients for the zero, first, second and third order polynomial can be found in Table 4.1. The fitting accuracy for the zero order polynomial is -9.28 dB, for the first order polynomial -9.97 dB, for the second order polynomial -21.01 dB and for

FIGURE 4.33: VNA Error Model for Calibration Standards

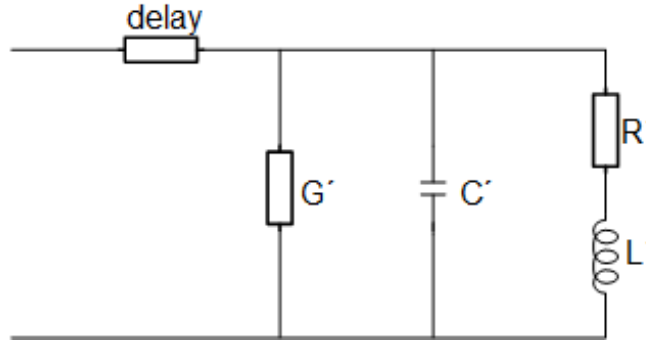TABLE 4.1: Short Calibration Standard Parameters

Order	$L_0\,[H/Hz^0]$	$L_1\,[H/Hz^1]$	$L_2\,[H/Hz^2]$	$L_3\,[H/Hz^3]$
0	58.035 E-12	-	-	-
1	74.642 E-12	-10219.931 E-24	-	-
2	141.689 E-12	-118632.251 E-24	33357.637 E-33	-
3	154.093 E-12	-153041.759 E-24	58074.651 E-33	-5070.157 E-42

TABLE 4.2: Open Calibration Standard Parameters

Order	$C_0\,[F/Hz^0]$	$C_1\,[F/Hz^1]$	$C_2\,[F/Hz^2]$	$C_3\,[F/Hz^3]$
0	62.965 E-15	-	-	-
1	95.683 E-15	-20133.818 E-27	-	-
2	92.116 E-15	-14367.038 E-27	-1774.394 E-36	-
3	96.181 E-15	-25642.631 E-27	6325.083 E-36	-1661.431 E-45

the third order polynomial -21.68 dB. The calculated parameter for the resistor is 1.87828 E-2 Ω.

- **Calculation of Open Parameters**

  Using the Y-parameters, because the parasitic capacitances are parallel to the ideal open, the coefficients for the open standard can be extracted. As for the short standard, different orders for polynomial describing the parasitic capacitances (Figure 4.35) are extracted. The Table 4.2 shows the results of the extraction. The fitting accuracy for the zero order polynomial is -12.09 dB, for the first order polynomial -28.86 dB, for the second order polynomial -29.73 dB and for the third order polynomial -30.16 dB. The calculated resistor value is 8.960673 E+03 Ω.

- **Calculation of Match Parameters**

  The coefficients for the polynomial describing the parasitic inductances of the match standard are extracted using the Z-parameters again. Only the parasitic inductances are extracted because they have more influence on the match as the parasitic capacitances. The results are shown in the Table 4.3. The fitting accuracy

TABLE 4.3: Match Calibration Standard Parameters

Order	$L_0\,[H/Hz^0]$	$L_1\,[H/Hz^1]$	$L_2\,[H/Hz^2]$	$L_3\,[H/Hz^3]$
0	247.106 E-12	-	-	-
1	193.803 E-12	32802.074 E-24	-	-
2	130.844 E-12	134603.255 E-24	-31323.440 E-33	-
3	94.991 E-12	234069.062 E-24	-102771.652 E-33	14656.043 E-42

for the zero order polynomial is -17.66 dB, for the first order polynomial -22.07 dB, for the second order polynomial -29.28 dB and for the third order polynomial -31.9 dB. The calculated resistor coefficient is 5.016759 E+01 Ω.

The fitting accuracy for the short inductance, the open capacitance and the match inductance for the third order polynomials are shown in Figures 4.34, 4.35 and 4.36.
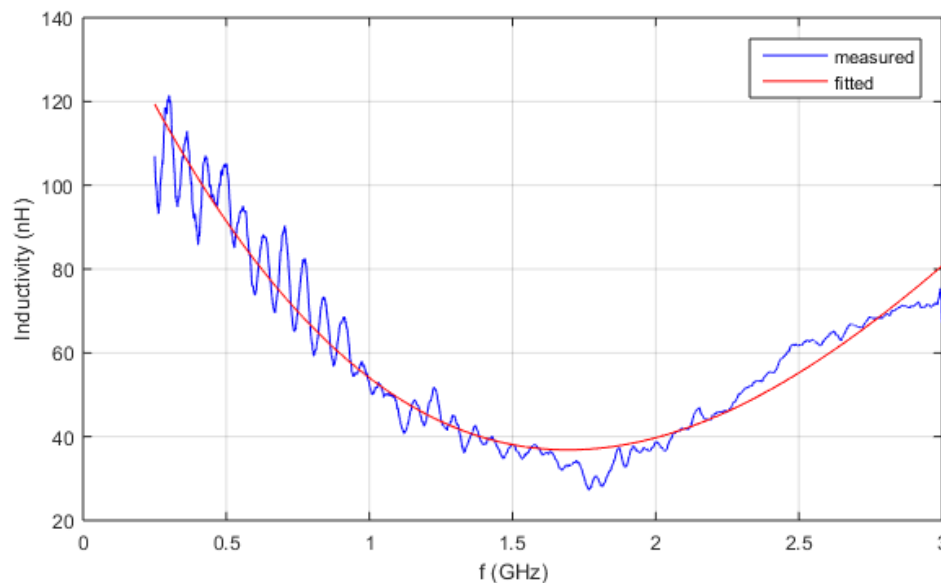

FIGURE 4.34: Fitting Accuracy for the Third Order Short Polynomial

4.5.3 Comparison of different Sets of Calibration Standard Coefficients

The parameters of the different calibration elements presented in Section 4.5.2 are needed to improve the accuracy of the corresponding VNA calibrations. Note that for the match and short standard the parasitic capacitances are assumed to be infinite and for the open standard the parasitic resistor is also assumed to be infinite.

The used calibration elements (Figures 4.5 and 4.8) are always the same but the order of the polynomial can be changed for each device individually. For example a calibration standard could be created using only zero order polynomial for the match standard,
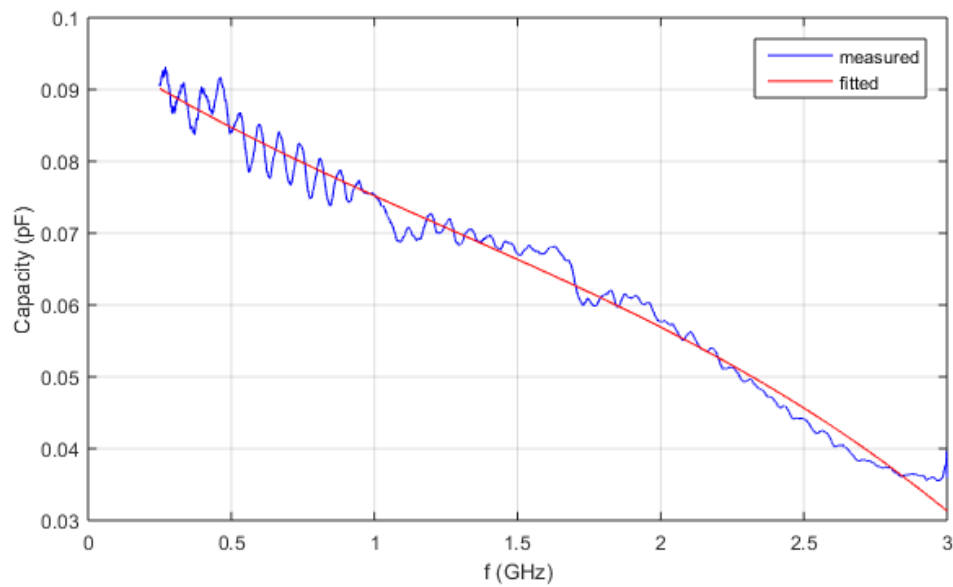
FIGURE 4.35: Fitting Accuracy for the Third Order Open Polynomial
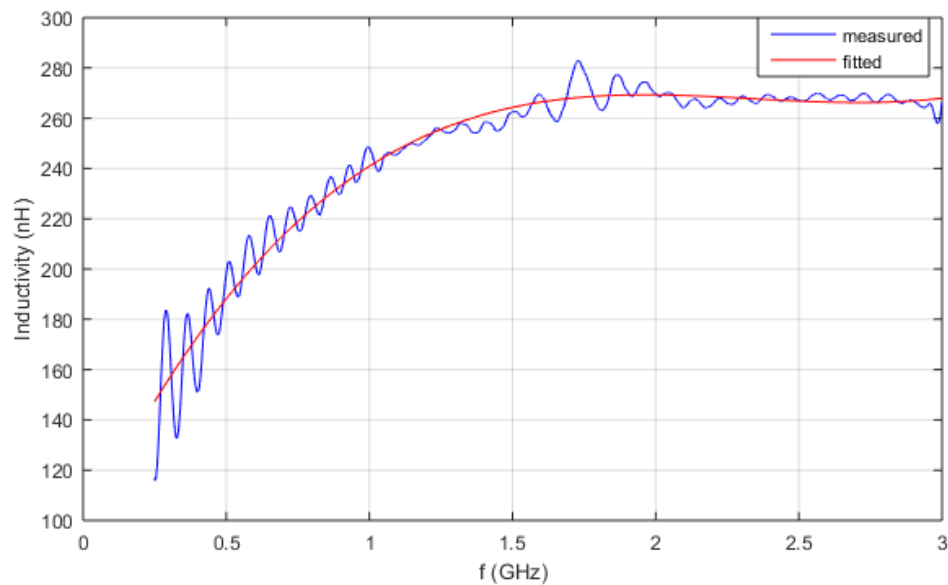
FIGURE 4.36: Fitting Accuracy for the Third Order Match Polynomial

but a second order polynomial for the open and a third order polynomial for the short standard. Looking at the fitting accuracy it can be decided which order is useful and if it is necessary to increase the order or stay at the lower one. Increasing the order of the polynomial for the short standard from two to three, only increases the fitting accuracy by 0.61 dB for example.

The example described above would be denoted as Meas O2S3M0 to be able to distinguish the different measurement sets. O stands for Open, S for Short and M for Match. The number next to it describes the order of the calibration standard polynomial. For

the case that all calibration standards use the same order, simply Meas Order 1 is written.

Taking the de-embedded measurement of the line 3 and the coil (VNA is calibrated with the manufacturer calibration-kit) as reference and changing the order of the polynomial of each calibration standard, the different sets of calibration standard coefficients can be compared.

The Figure 4.37 shows the results for the line 3 and Figures 4.38 and 4.39 the results for the coil. Note that for these figures a smoothing factor is used for a better representation of the results. Because of a good enough matching of the line 3, only the transmission parameters (S_{21}, S_{12}) are compared. The matching is always below -30 dB which means that measurement errors have a greater influence on the results and that the values are too small for a representative comparison analysis.

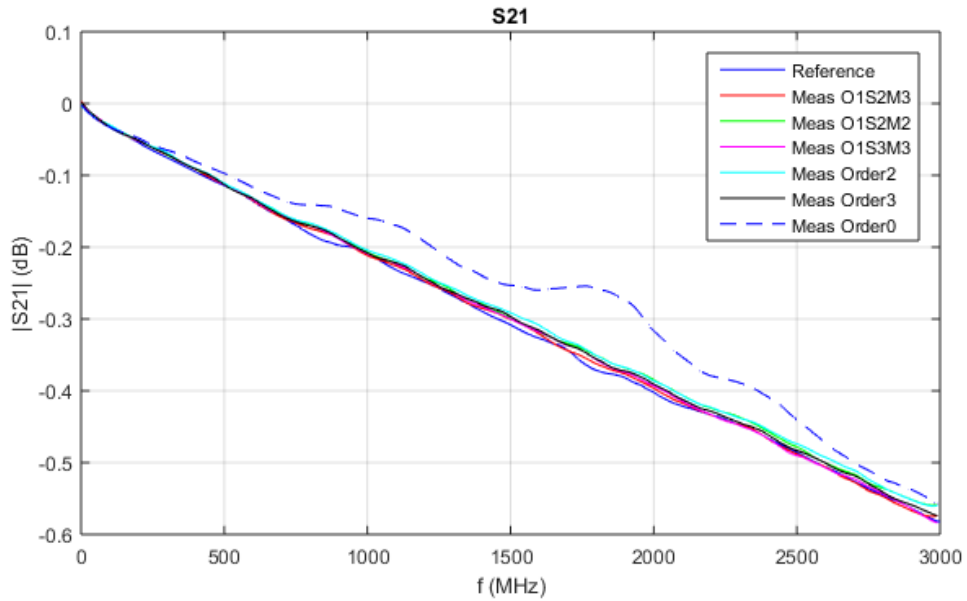For the coil all S-parameters are compared to the reference measurement.

FIGURE 4.37: Comparison of different Sets of Calibration Standards for Line 3 S_{21}

The results for the transmission S_{21} are coherent with the reference measurement except for the zero order set of calibration coefficients. To get the best set (least complex and least deviation from the reference measurement) the Figure 4.37 is not very representative. Therefore the error e between the selected measurement and the reference measurement is introduced (Equation 4.13).

$$e\big|_{dB} = 20 \cdot log_{10} \frac{\sum(|S_{meas} - S_{ref}|^2)}{\sum(|S_{ref}|^2)} \tag{4.13}$$

To get one parameter for the reflection error (Γ_{error}) and one for the transmission error (τ_error), a weighing of the error values is done (Equation 4.14).
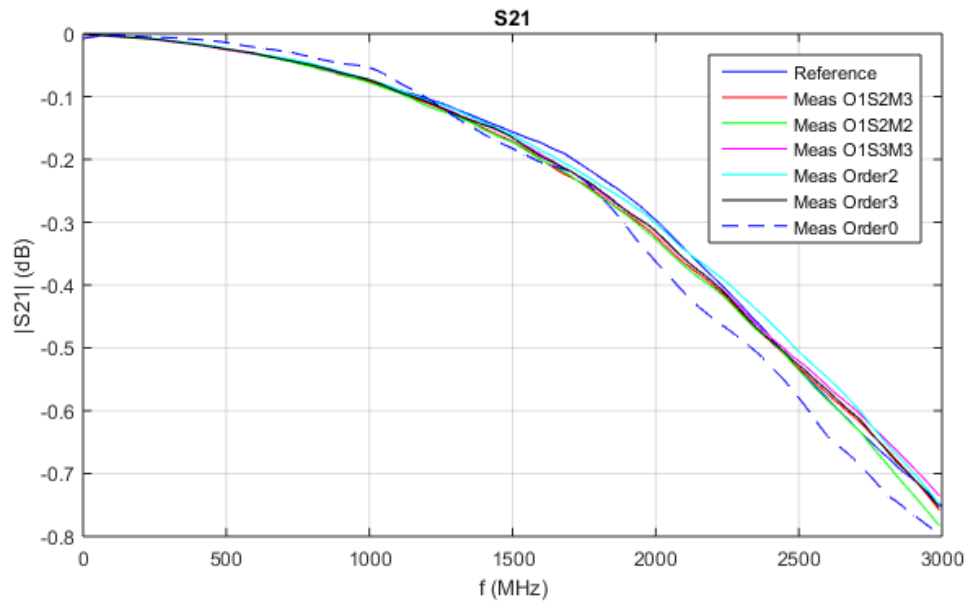
FIGURE 4.38: Comparison of different Sets of Calibration Standards for the Coil S_{21}
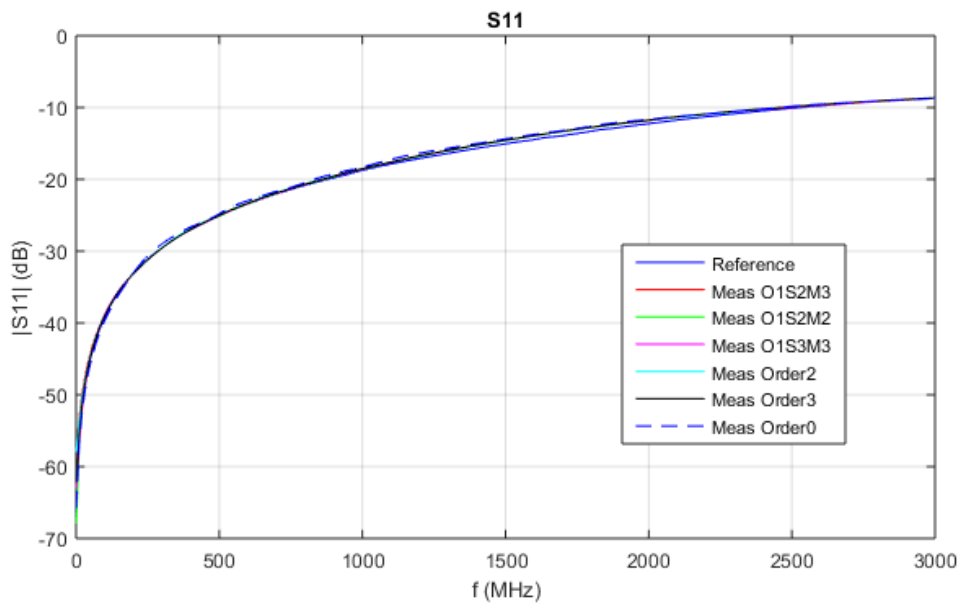
FIGURE 4.39: Comparison of different Sets of Calibration Standards for the Coil S_{11}

$$\Gamma_{error}\big|_{dB} = 0.5 \cdot e_{11} + 0.5 \cdot e_{22}$$
$$\tau_{error}\big|_{dB} = 0.5 \cdot e_{21} + 0.5 \cdot e_{12}$$

$$(4.14)$$

The Tables 4.4 and 4.5 show the errors calculated for the coil and the line 3 measurement.

The conclusion for the comparison of the different calibration sets for the coil measurement is that the set with a polynomial order of one for the open standard, two for the

TABLE 4.4: Error Parameters for Coil Measurement

	$\Gamma_{error}[dB]$	$\tau_{error}[dB]$
Order 0	-38.4	-65.66
Order 2	-51.95	-83.97
Order 3	-53.29	-84.75
O1S2M2	-52.62	-81.56
O1S2M3	-56.46	-84.03
O1S3M3	-56.77	-82.81

TABLE 4.5: Error Parameters for Line 3 Measurement

	$\tau_{error}[dB]$
Order 0	-59.79
Order 2	-83.49
Order 3	-79.1
O1S2M2	-75.52
O1S2M3	-81.76
O1S3M3	-79.67

TABLE 4.6: Coefficient of the O1S2M3 Set

Order	0	1	2	3
C_{Open}	95.683 E-15	-20133.818 E-27	-	-
L_{Short}	141.689 E-12	-118632.251 E-24	33357.637 E-33	-
L_{Match}	94.991 E-12	234069.062 E-24	-102771.652 E-33	14656.043 E-42

short standard and three for the match standard (O1S2M3) appears to result in the best performance.

Since the transmission error is below -75 dB for every set and also measurement except the zero order set, the set O1S2M3 is chosen to define the custom calibration-kit (Table 4.6).

Chapter 5

Planar Structures at 74GHz

This chapter has its focus on the possibilities to measure and analyze planar structures at 74 GHz for a mm-wave RFID transponder (Figure 5.1). The elements that need to be analyzed at 74 GHz are the antenna, the matching network, the low-pass filter and the mm-wave diode. However in order to do so launches have to be designed to be able to measure the DUTs with a VNA. Since this thesis is only a part of the project to build a mm-wave RFID demonstrator, it will solely focus on the launches to connect the DUTs with the VNA. Such a launch should have a good matching and as low transmission losses as possible to minimize the measurement errors.
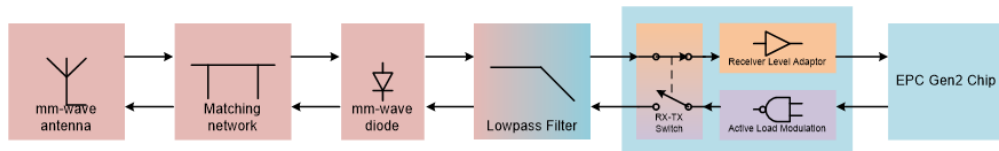

FIGURE 5.1: Block diagramm of the mm-wave RFID Transponder [6]

Measurements at mm-wave frequencies are more complicated than the measurements done in Chapter 4. One approach would be to find a suitable coaxial mm-wave connector and connect the DUT with the VNA as done in Chapter 4. Another approach is to use a probe station. The problem with the first approach is, that these connectors are very expensive and not built to be switched between circuit boards very often although they are not soldered onto them but just screwed onto the circuit boards. The second approach is much more suitable to test more circuit boards containing the same structures, although the initial costs for this kind of system are rather high. These planar structures have to be tested multiple times on different boards to verify the results and to be able to characterize the microwave elements.

Despite of the fact that more structures were investigated, in the framework of this thesis the attention is put to the treatment of the launches. That is the name of the area

where the coaxial connector is screwed onto respectively where the probe station has its touchdown.

All simulated structures have a characteristic impedance of $75\,\Omega$. This value is chosen to minimize the line width and gap size for a grounded co-planar wave-guide to enable a touchdown for a $150\,\mu$m probe station probe-size, while maintaining producibility. Another benefit is the higher voltage level, compared to a $50\,\Omega$ structure which is crucial for the actual application afterwards.

A different aspect, that has to be reconsidered when testing planar structures, is the fabrication process itself. Figure 5.2 shows the stack-up (the different layers of a PCB) of the PCB fabricated by AT&S. This manufacturer allows a minimal track width of $50\,\mu$m and a minimal distance of $50\,\mu$m between two copper structures. The minimal via size is $175\,\mu$m with a minimal restring of $100\,\mu$m. These are the so called design rules which indicate the smallest element the manufacturer can fabricate. In order to get the best performance of the launch of the probe station, these design rules are pushed to their limits respectively are violated, which causes AT&S to use a different fabrication process.

FIGURE 5.2: Stack-up of the AT&S Circuit Board

Unfortunately the cross section of any realized transmission line is not a perfect rectangular but rather a trapezoid due to the etching process, which results in an undercut (see Figure 5.3). Since planar structures have rather thin transmission lines for thin substrates, this effect has to be reconsidered in the simulation. The model shown in Figure 5.3 is a simplification to minimize the simulation time. For a full re-modeling of the cross section, the nickel and gold layers have to be extended to cover the copper layer not only on the top but also on the sides of the trapezoid.

The goal of these simulations is to find a launch that enables the measurement and characterization of different planar structures at $74\,$GHz. A suitable connector has a good matching ($S_{11} < $ -25 dB) and low transmission loss ($S_{21} <<$) over a wide frequency range. That is why the simulations for the launch for the probe station are run from
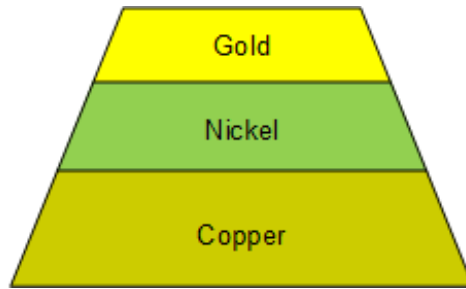
FIGURE 5.3: Crosssection of a real Transmission Line

1 GHz up to 90 GHz. The frequency range covered by the simulations for the mm-wave Coaxial Connector is also from 1 GHz to 90 GHz.

5.1   mm-wave Coaxial Connector

The used connector is the 1 mm End Launch Connector from Southwest Microwave. To get good simulation results the connector is drawn in the CST-tool (Computer Simulation Technology) and then used as the feeding port for the planar structures. Figure 5.4 shows the modeled connector in CST on a circuit board with a micro-strip line structure.
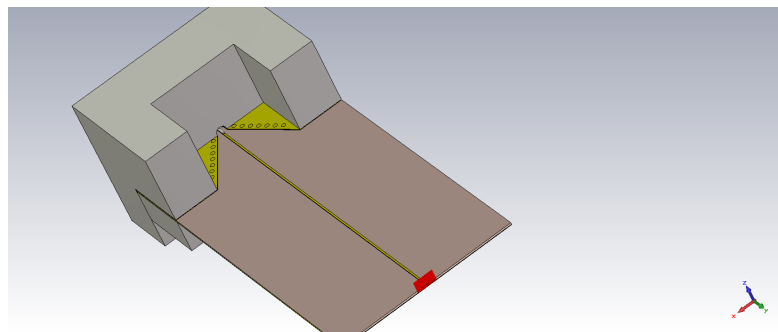

FIGURE 5.4: Simulation Model of the Coaxial Connector

For this approach the transition area (see Figure 5.5) from a coaxial waveform mode to a micro-strip mode is modified. Figure 5.5 shows the manufacturers recommendation on the left and a variant of the recommendation on the right hand side. The idea is to create a smooth transition and not an abrupt one. This is done by adding triangular ground planes.

As mentioned before, the micro-strip line has a characteristic impedance of 75 Ω, but the connector is optimized for 50 Ω. Therefore a matching technique, called the $\lambda/4$ transformer (Figure 5.7) is also tested to achieve an optimal input matching as well as a low transmission loss.
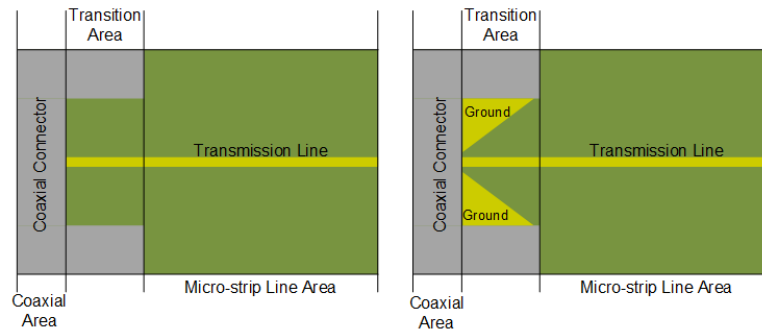
FIGURE 5.5: Variants of the Transition Area for Coaxial Connector

5.1.1 Simulation Results

- **Comparison Smooth to Abrupt Transition**

  The coaxial connector has a good matching for a very selective frequency band (see Figure 5.6). Expanding the ground planes, as shown in Figure 5.5 results in a better matching at 74 GHz. The frequency point of interest.
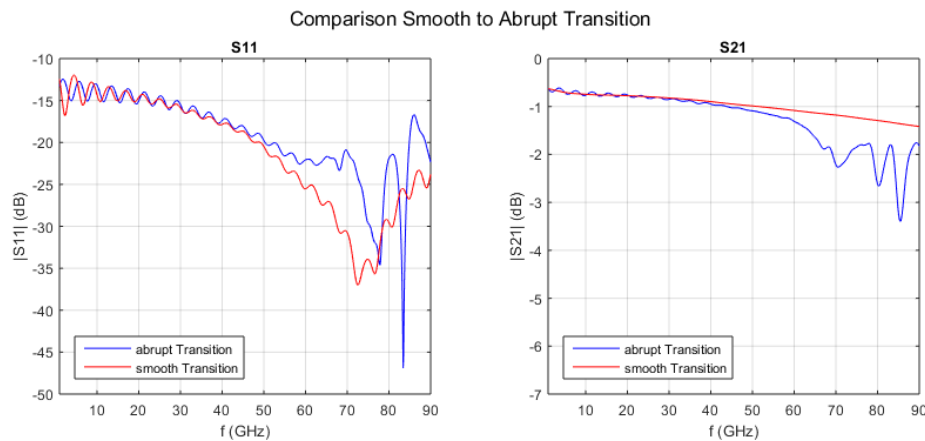

FIGURE 5.6: Comparison of the S-Parameters for Smooth and Abrupt Transition

  Furthermore the transmission coefficient S_{21} also shows an improved performance for a smooth transition. Also the highly resonant behavior starting at 60 GHz up to 90 GHz can be removed completely. For this simulation the model shown in Figure 5.4 is used. This model has only one End Launch connector and ends the micro-strip line at port 2.

- **Comparison $\lambda/4$ Transformer to Direct Transition**

  The Figure 5.8 compares the S-parameters for an excitation of port one of a direct transition and a transition using a $\lambda/4$ transformer (Figure 5.7).

  Although the expected performance of a transition with a $\lambda/4$ transformer is supposed to be better, the simulation shows that a direct transition has a less resonant
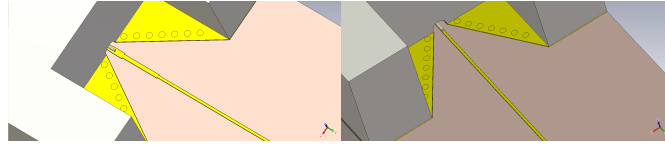
FIGURE 5.7: Model of the Coaxial Connector with and without a $\lambda/4$ Transformer
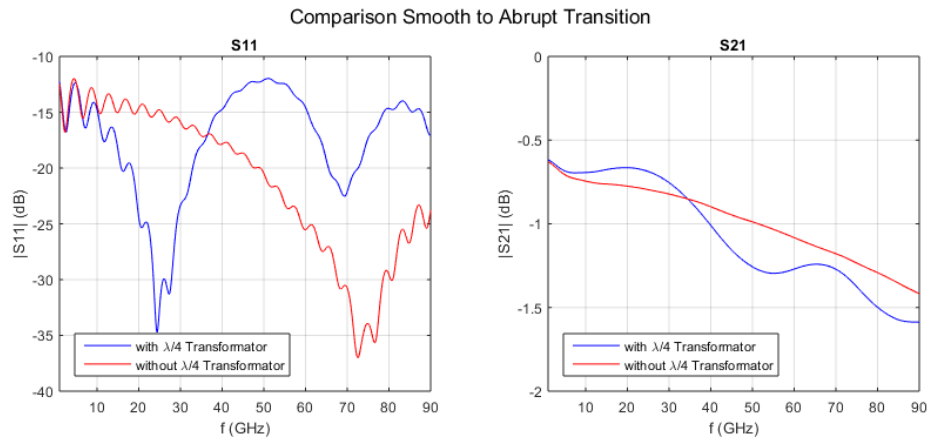
FIGURE 5.8: Comparison of $\lambda/4$ Transformer to Direct Transition, S_{11} and S_{21}

behavior and in general a better matching and transmission for the desired frequency range. It also shows that optimizing the $\lambda/4$ transformer would result in an equally good matching, but such a transformer always results in a narrow band system which is not desired for this case.

- **Through Arrangement**

  Figure 5.9 shows the model of a through circuit board using two coaxial connectors. The length of the circuit board is 25.4 mm.
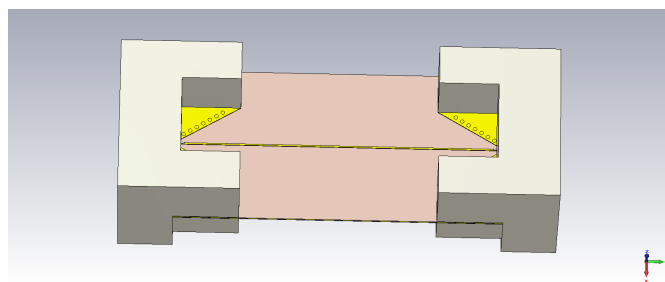
FIGURE 5.9: Two Coaxial Connectors in a Through Arrangement

This arrangement is also used to measure different line lengths. Line 1 is 20.15 mm, line 2 is 20.3 mm and line 3 is 20.45 mm long. The results can be seen in Figure 5.10.

The measurement results indicate much higher losses than predicted by the simulation. This fact alone is not surprising since that could mean, that the simulation did not take all the material properties into account. The unusual part of the

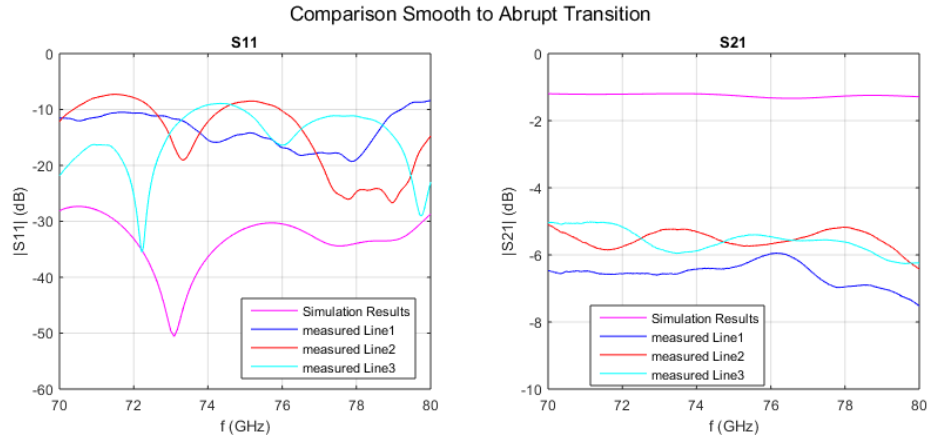FIGURE 5.10: Simulation and Measurement Results of the Coaxial Connector in a Through Arrangement

measurement results is, that the shorter line 1 shows higher insertion losses than the longer line 3. This indicates that the measurement results are influenced by the way the coaxial connectors are mounted, which leads to uncertainties that can not be neglected.

5.1.2 Conclusion

The simulations show that a design with a smooth transition and no $\lambda/4$ transformer yields the best results. Figure 5.11 displays the designed launch for the mm-wave coaxial connector.
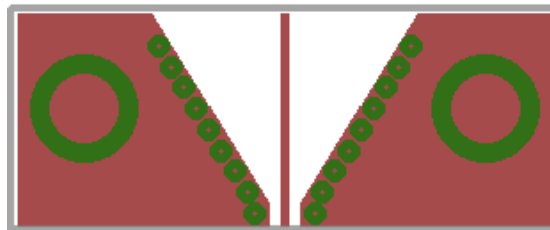
FIGURE 5.11: Design of the mm-wave Coaxial Connector

Subsequently the coaxial end launch connector showed too many uncertainties, that influence the measurement results to use it for further analysis of the other planar structures that are part of the mm-wave RFID transponder. Examples for these uncertainties are the tightness of the screws and if the connector is centered or not. Another uncertainty is, if a good connection between connector and circuit board is established or not.

5.2 Launch for Probe Station

The launch for a probe station has to make two transitions between wave-forms. From a co-planar wave-guide mode (excited by the probe station, CPW) to a grounded co-planar wave-guide (GCPW) mode and finally to a micro-strip line mode. Therefore it is vital that a good ground connection between the top layer ground polygons and the bottom layer ground is established. Since the vias have a certain length they can not be considered as an ideal short circuitry at mm-wave frequencies. Hence the positioning of the vias is an important parameter that has to be examined for a good matching and transmission of the launch to the probe of the probe station.

The launch consists of a GCPW area, a transition area from the GCPW mode to a micro-strip line mode and the micro-strip line mode area (Figure 5.12). Both, GCPW and the micro-strip line are designed for $75\,\Omega$ (a = width of GCPW transmission line with gap size b, c = width of micro-strip line).

Besides the positioning of the vias and the different lengths of the areas, the distance ($trans_d$) between the transmission line at the end of the transition area and the ground plane has also an influence on the characteristics of the launch (Figure 5.12).
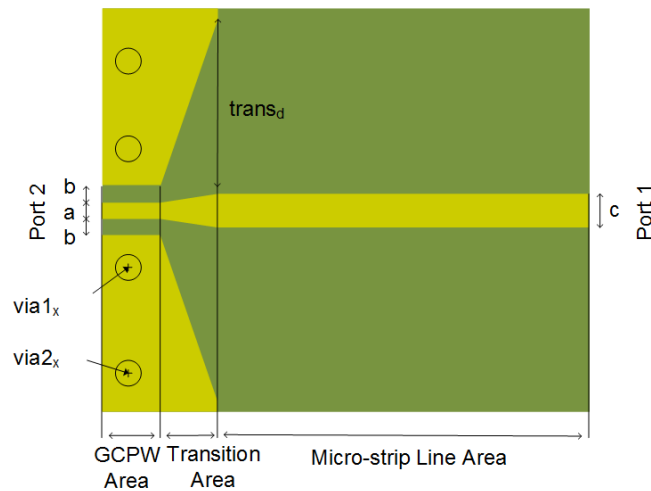

FIGURE 5.12: Model of the Launch for the Probe Station

5.2.1 Simulation Results

The lengths of the GCPW area and the micro-strip line area are kept constant for the simulation. They should be kept as short as possible to minimize losses at the launch. On the other hand they have to have at least a certain length for the modes to develop.

- **Influence of the Distance of the Ground Plane ($trans_d$) and the Length of the Transition Area ($trans_l$)**

  With a constant GCPW length of $0.3\,\text{mm}$ and a micro-strip line length of $1\,\text{mm}$ the length of $trans_l$ is changed in $0.05\,\text{mm}$ steps from $0.2\,\text{mm}$ to $0.5\,\text{mm}$. The two vias are placed at $via1_x = via2_x = 0.15\,\text{mm}$, $via_d = 0.4\,\text{mm}$ and $via_{diff} = 0.6\,\text{mm}$. The length of the GCPW area is chosen to be $0.3\,\text{mm}$ to allow the GCPW mode of the signal to develop itself, but also to minimize the losses (this parameter was optimized in an initial simulation run).

  The parameter $trans_d$ is also changed in $0.05\,\text{mm}$ steps from $0.4\,\text{mm}$ to $1.15\,\text{mm}$ (this is the maximal distance because of the chosen width of the launch).

  Port 2 is exciting the launch. That is why the S-parameters S_{22} and S_{12} are more important for the design decisions and shown in the following figures. All contour plots are presented for a frequency range from $1\,\text{GHz}$ to $90\,\text{GHz}$.
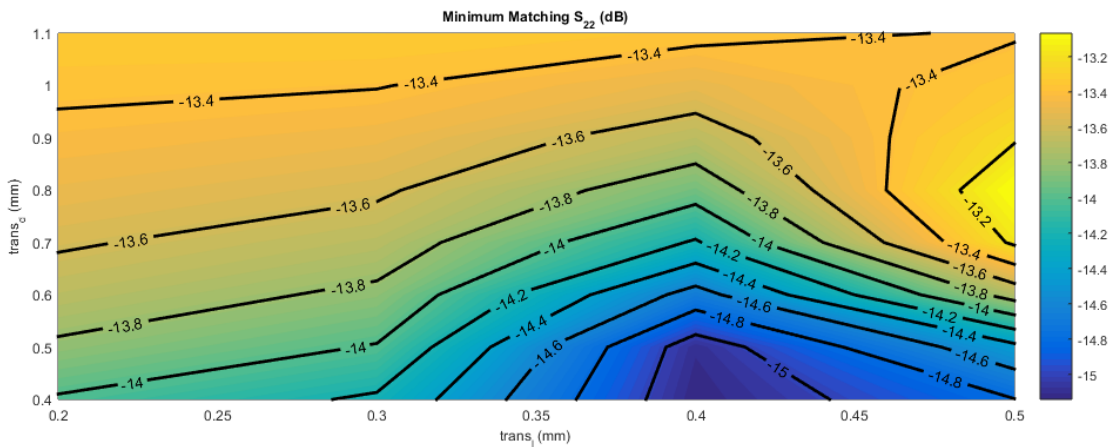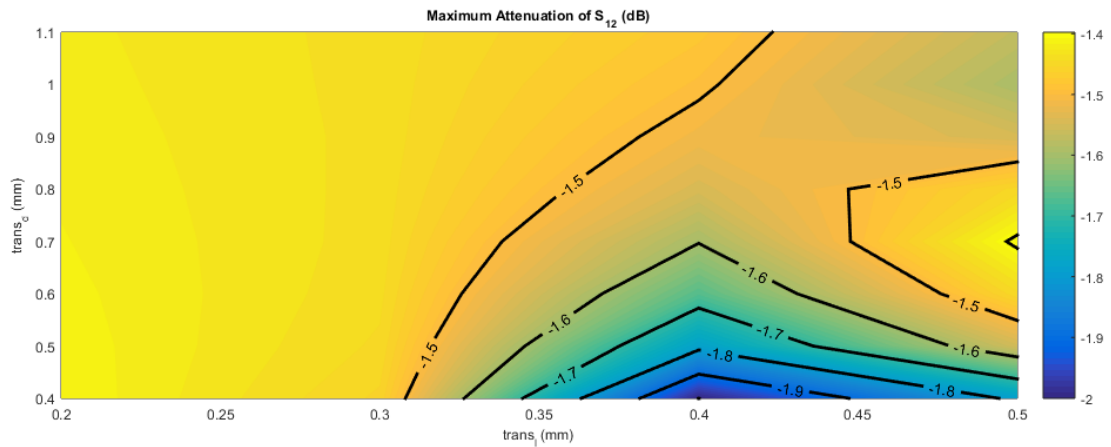

FIGURE 5.13: Simulation Results S_{22}

As the Figures 5.13 and 5.14 show, that the matching increases for a decreasing $trans_d$ and reaches a maximum for $trans_l = 0.4\,\text{mm}$. However the insertion losses are decreasing for a shorter $trans_l$.

A transition length of $0.3\,\text{mm}$ and $trans_d$ being at its maximum ($1.15\,\text{mm}$) lead to the best performance of the launch within the chosen parameters.

- **Varying the Vias Positions**

  After having set the optimal transition length and $trans_d$, the vias positions are

FIGURE 5.14: Simulation Results S_{12}

changed. Starting with only one via, the optimal distance from the via to the transmission line (via_d) is evaluated. Therefore the via is moved from the closest possible point that is still within the ground plane, to the farthest point possible (Figure 5.15). The position is only changed in the vertical direction, assuming the orientation of the launch as it is in Figure 5.12. The parameter-sweep of via_d runs from 0.25 mm to 1 mm with a step-size of 0.05 mm.
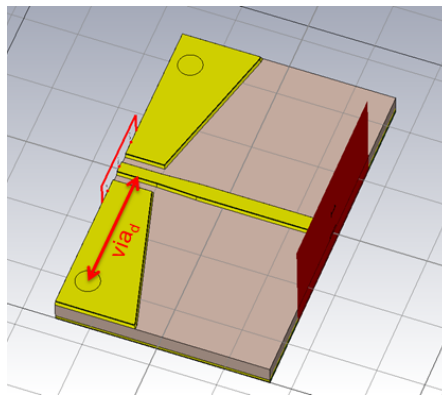

FIGURE 5.15: Simulation Model for the Variation of the Position of one Via

Compared to the variation of the transition length, the positioning of the vias has an even greater impact on the performance of the launch. The optimum of the vertical position is obtained for a distance of the first via to the transmission line (via_d) of 0.35 mm.

Using one via leads to a good matching in general (Figure 5.16) for a certain via position where the parasitic inductances have a positive influence on the launch matching and transmission.

Figure 5.17 shows the simulation runs with a second via. Adding a second via increases the number of the possible parameter sweeps significantly. The Figures 5.18, 5.19, 5.20 and 5.21 show the variation of the vertical and horizontal positions
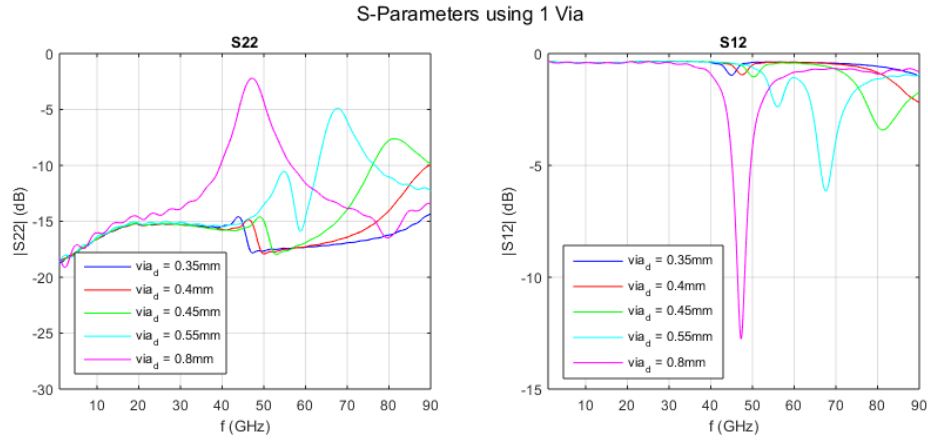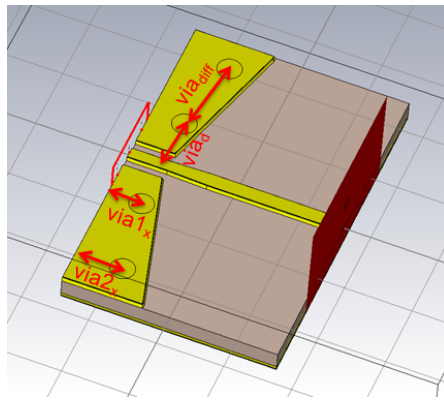
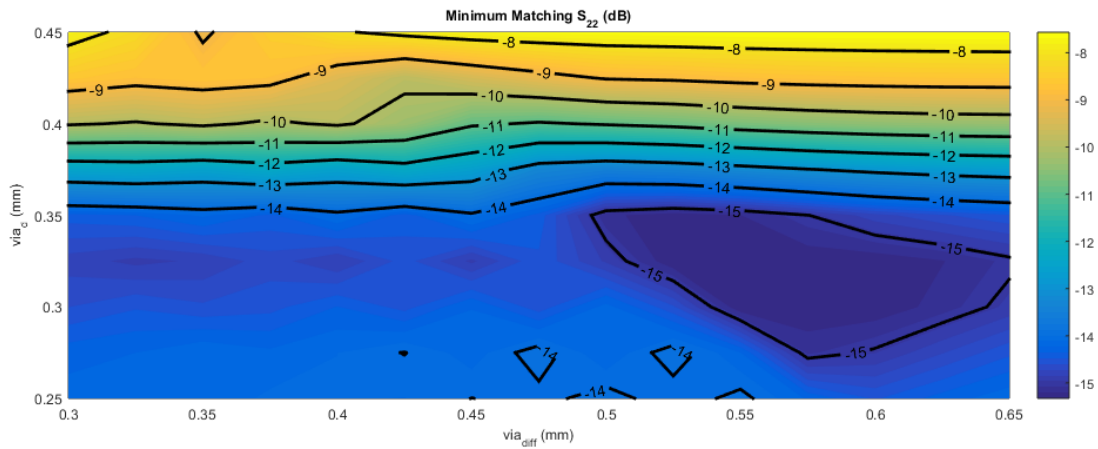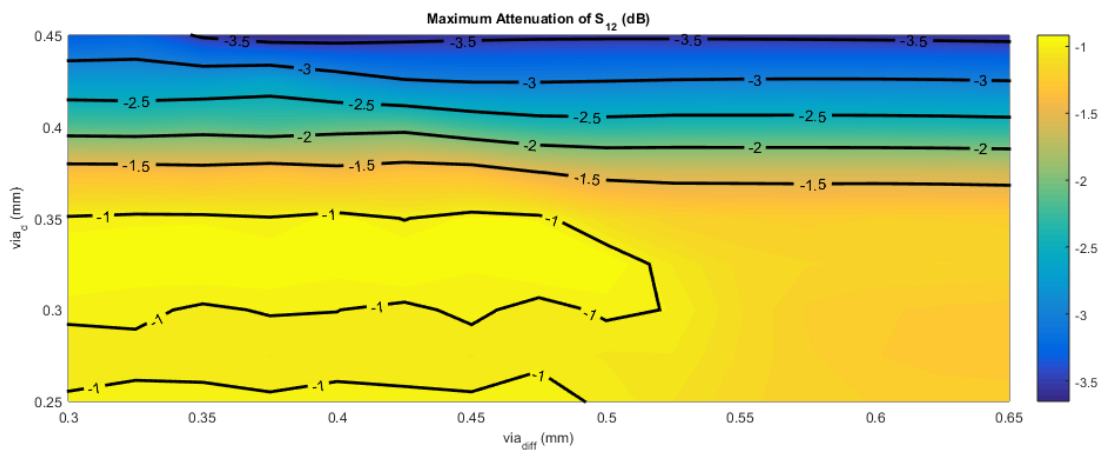FIGURE 5.16: Simulation Results S_{22} and S_{12} for one Via

FIGURE 5.17: Simulation Model for the Variation of the Position of two Vias

of the vias.

For the vertical position the changed parameters are via_d and via_{diff}, which describe the distance of the vias to the transmission line and the space in between the vias respectively. via_d ranges from 0.25 mm to 0.45 mm and the range of via_{diff} is from 0.3 mm to 0.65 mm. The parameter $via1_x$ denotes the distance of the center of the first via to the left edge of the launch. $via2_x$ does the same for the second via. $via1_x$ ranges from 0.10 mm to 0.25 mm and the range of $via2_x$ is from 0.10 mm to 0.35 mm. All parameters are changed with a step size of 0.05 mm.

The Figures 5.18, 5.19, 5.20 and 5.21 contain the results for a frequency sweep between 1 GHz and 90 GHz. In this frequency band the worst case scenario for the matching and transmission is compared, depending on the position. That means the maximum value for the matching and the minimum value for the transmission is chosen.

For the variation of the vertical positions of the two vias, values for via_d below 0.4 mm show the best results while the variation of via_{diff} has a minimal influence on the performance (Figures 5.18 and 5.19).

FIGURE 5.18: Simulation Results S_{22} for the Variation of via_d and via_{diff}

FIGURE 5.19: Simulation Results S_{12} for the Variation of via_d and via_{diff}
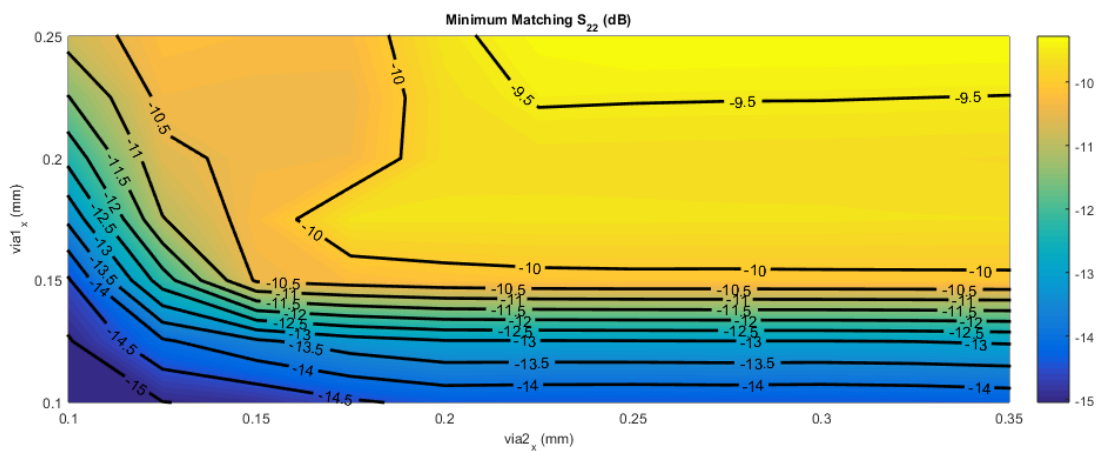
FIGURE 5.20: Simulation Results S_{22} for the Variation of $via1_x$ and $via2_x$

Changing the horizontal position (Figures 5.20 and 5.21) improves the performance of the launch. According to the contour plots the best results would be at $via1_x = 0.1\,\text{mm}$ and $via2_x = 0.25\,\text{mm}$. However, the placement of the vias in the optimal position pushes the limits of the design rules of the manufacturer. Therefore
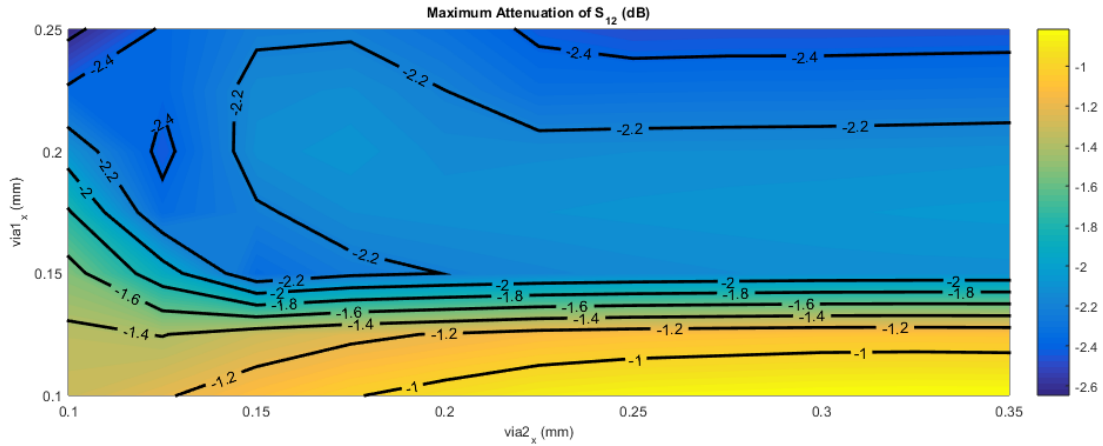
FIGURE 5.21: Simulation Results S_{12} for the Variation of $via1_x$ and $via2_x$

various designs are ordered, to test these limits and the launch that has the best performance without pushing the design rules too much is used as the connector between the probe station and the designed planar structures.

5.2.2 Conclusion of the Simulation Results

For the optimal design analysis, a behavioral analysis of the S-parameters over the frequency is required additionally to the contour plots. This investigations have been performed but are not shown within this thesis.

The compromise between performance and still fabricate-able design is displayed in Figure 5.22. This launch has a GCPW area length of 0.3 mm, a transition area length of also 0.3 mm and a micro-strip line area length of 1 mm. The distance between the transmission line and the ground plane at the end of the transition area is 1.15 mm. The vias are placed 0.15 mm away from the left edge of the launch and at a distance (via_d) of 0.4 mm from the center of the transmission line with a separation (via_{diff}) of 0.6 mm to each-other (Table 5.1).

TABLE 5.1: Dimensions of the Realized Launch

GCPW length	Transition length	Micro-stip Line length	$trans_d$
0.3 mm	0.3 mm	1 mm	1.15 mm
$via1_x$	$via2_x$	via_d	via_{diff}
0.15 mm	0.15 mm	0.4 mm	0.6mm
GCPW width	Micro-strip Line width	Gap width	
0.11 mm	0.14 mm	0.055 mm	
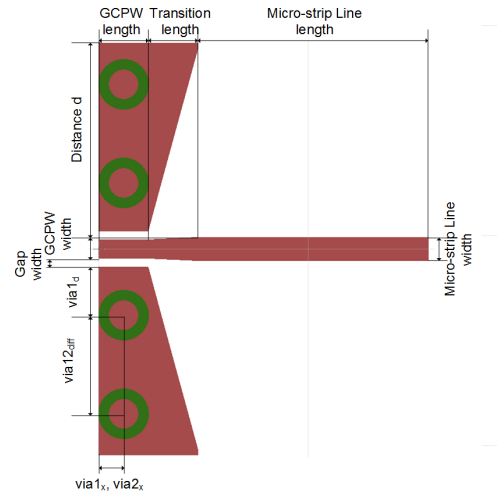
FIGURE 5.22: Layout of the used Launch

5.3 Measurement Results

Since the analysis of the performance of the launch needs two launches in a through arrangement to enable a measurement with the probe station, this structure is also simulated for a direct comparison between the simulation and measurement results. In Figure 5.23 the simulation model is shown.

FIGURE 5.23: Two Launches in a Through Arrangement

FIGURE 5.24: Comparison between the Measurement and Simulation

Figure 5.24 shows the comparison between the measured and simulated results. While the transmission coefficients show a good agreement up to 60 GHz, the measurements outperform the simulations.
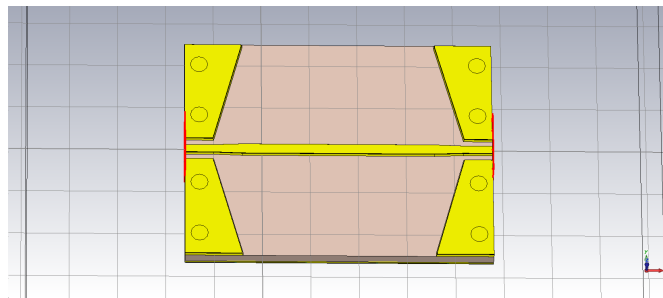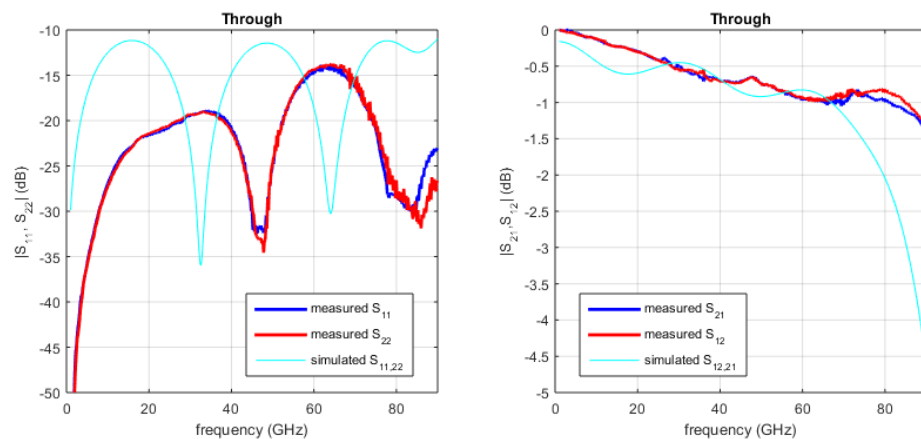
According to the measurement results the DUT appears to be electrically shorter than the simulation predicts. This can be deducted from the shift of the minima of the matching parameters (S_{11},S_{22}). The fact that the maxima of the matching parameters are not equally high leads to the conclusion, that there is a mismatch (different characteristic impedance) between the three areas, that is not included in the simulation. Furthermore the transition of the modes (GCPW to a micro-strip line) seems to be not as fast as predicted by the simulation, which would explain the shorter electrically length, because the modes are not yet fully developed.

5.4 Outlook

Since the first measurement results have shown a deviation to the simulation, six additional variants of the launch have been manufactured to improve the simulation model. The dimensions, respectively the parameters that are changed compared to the first prototype (Table 5.1) are presented in Table 5.2.

TABLE 5.2: Changed Parameters of the Launch Variants

	$via1_x$	$via2_x$	$via1_d$	Gap width
Variant 1	0.1 mm	0.25 mm	0.4 mm	0.055 mm
Variant 2	0.2 mm	0.1 mm	0.4 mm	0.055 mm
Variant 3	0.15 mm	0.15 mm	0.37 mm	0.055 mm
Variant 4	0.15 mm	0.15 mm	0.43 mm	0.055 mm
Variant 5	0.15 mm	0.15 mm	0.4 mm	0.05 mm
Variant 6	0.15 mm	0.15 mm	0.4 mm	0.055 mm

The sixth variant has the same dimensions as the launch shown in 5.22 but adds a bridge between the two top ground planes (see Figure 5.25). This bridge has a width of 0.11 mm and the gap size is also 0.055 mm.

The measurements of the additional prototypes are currently being conducted and evaluated. The results of these investigations will be presented in [11].
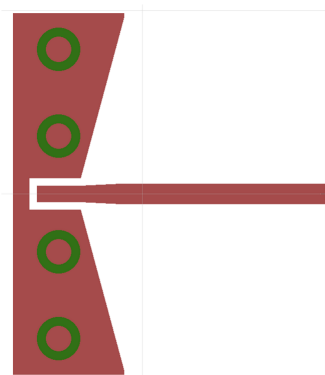

FIGURE 5.25: Layout of the sixth Variant

Chapter 6

Conclusion

Within this thesis a custom-built SOLT calibration-kit for GCPW interfaces and a test fixture for the probe station were designed and verified. For the SOLT calibration-kit the focus was put on easy and low cost producibility while maintaining a reasonable performance up to 3 GHz. The attention for the interface for the probe station was paid on low insertion losses and a non-resonant broadband behavior from DC to 90 GHz.

6.1   SOLT Calibration-kit

The SOLT calibration-kit enables the analysis of various components with different pad sizes up to 3 GHz. To improve the accuracy of the VNA error model (Figure 4.33) polynomials of different degrees were extracted and evaluated for the match, short and open equivalent models.

A comparison with a commercially available calibration-kit was performed. The de-embedded results were taken as a reference for the performance of the custom-built SOLT calibration-kit. The error between the reference and the SOLT calibrated measurement is less than -75 dB.

6.2   Launch

The performance of the designed launch exceeds the simulation results. The measurement shows that a matching below -15 dB is obtained over the whole frequency range for a through arrangement where two launches are directly connected to each other. Furthermore the insertion losses are below 1 dB up to 80 GHz and a non-resonant broadband behavior over the whole frequency range is also accomplished.

6.3 Future Work

To increase the accuracy of the SOLT calibration-kit even further, a deeper look into the de-embedding process has to be done. This will also benefit the analysis done for the components at mm-wave frequencies.

For the launch the measurements of the six variants have to be evaluated and compared with the simulation. This work will be shown in [11]. Furthermore these outcomes will be used to improve the simulation model. Additionally the probe tips should be included in the simulations.

Bibliography

[1] K. Finkenzeller, *RFID Handbook Fundamentals and Application in Contactless Smart Cards, Radio Frequency Identification and Near- Field Communication, Third Edition.* John Wiley & Sons, 2010.

[2] Y. Rahmat-Samii, L. I. Williams, and R. G. Yoccarino, "The UCLA Bi-polar Planar-Near-Field Antenna Measurement and Diagnostics Range," *IEEE Antennas and Propagation Magazine Vol. 37, No. 6*, 1995.

[3] D. M. Pozar, *Microwave Engineering.* Wiley, 2012.

[4] M. Gadringer, "RF Measurement Lab Vektor Netzwerk Analysator," 2013.

[5] M. Hiebel, "Vector Network Analyszer (VNA) Calibration: The Basics."

[6] P. F. Freidl, M. E. Gadringer, U. Mühlmann, G. Holweg, and W. Bösch, "A mm-Wave RFID System based on the EPC-Gen2 Protocol," in *Proceedings of the 2015 IEEE AP-S Symposium on Antennas and Propagation and URSI CNC/USNC Joint Meeting*, 2015.

[7] P. Young, "Scattering coefficients and circuit analysis," *The 14th IEE Microwave Measurements Training Course*, May 2005.

[8] H. Heuermann, *Hochfrequenztechnik*, 2nd ed. Vieweg+Teubner Verlag, 2009.

[9] D. Rytting, "Network Analyzer Error Models and Calibration Methods," -.

[10] B. C. Wadell, *Transmission Line Design Handbook.* Artech House, Inc., 1991.

[11] P. F. Freidl, S. W. Sattler, D. Amschl, M. E. Gadringer, U. Mühlmann, G. Holweg, and W. Bösch, "Design of PCB RF Probe Landing Pads for Measurements Up to 90 GHz," in *Proceedings of the 10th European Conference on Antennas and Propagation (EuCAP), submitted*, 2016.